Remote effects of Tibetan Plateau spring land temperature on global subseasonal to seasonal precipitation prediction and comparison with effects of sea surface temperature: the GEWEX/LS4P Phase I experiment

Yongkang Xue[1] · Ismaila Diallo[1,31] · Aaron A. Boone[2] · Yang Zhang[3] · Xubin Zeng[4] · William K. M. Lau[5] · J. David Neelin[1] · Tandong Yao[6] · Qi Tang[7] · Tomonori Sato[8] · Myung-Seo Koo[9] · Frederic Vitart[10] · Constantin Ardilouze[2] · Subodh K. Saha[11] · Stefano Materia[12,13] · Zhaohui Lin[14] · Yuhei Takaya[15] · Jing Yang[16] · Tetsu Nakamura[8] · Xin Qi[16] · Yi Qin[7,17] · Paulo Nobre[18] · Retish Senan[10] · Hailan Wang[19] · Hongliang Zhang[20] · Mei Zhao[21] · Hara Prasad Nayak[1] · Yan Pan[3] · Xiaoduo Pan[6] · Jinming Feng[14] · Chunxiang Shi[22] · Shaocheng Xie[7] · Michael A. Brunke[4] · Qing Bao[23] · Marcus Jorge Bottino[18] · Tianyi Fan[16] · Songyou Hong[9,24] · Yanluan Lin[17] · Daniele Peano[12] · Yanling Zhan[14] · Carlos R. Mechoso[1] · Xuejuan Ren[3] · Gianpaolo Balsamo[10] · Sin Chan Chou[18] · Patricia de Rosnay[10] · Peter J. van Oevelen[25] · Daniel Klocke[26] · Michael Ek[27] · Xin Li[6] · Weidong Guo[3] · Yuejian Zhu[19] · Jianping Tang[3] · Xin-Zhong Liang[28] · Yun Qian[29] · Ping Zhao[30]

Abstract

The prediction skill for precipitation anomalies in late spring and summer months—a significant component of extreme climate events—has remained stubbornly low for years. This paper presents a new idea that utilizes information on boreal spring land surface temperature/subsurface temperature (LST/SUBT) anomalies over the Tibetan Plateau (TP) to improve prediction of subsequent summer droughts/floods over several regions over the world, East Asia and North America in particular. The work was performed in the framework of the GEWEX/LS4P Phase I (LS4P-I) experiment, which focused on whether the TP LST/SUBT provides an additional source for subseasonal-to-seasonal (S2S) predictability. The summer 2003, when there were severe drought/flood over the southern/northern part of the Yangtze River basin, respectively, has been selected as the focus case. With the newly developed LST/SUBT initialization method, the observed surface temperature anomaly over the TP has been partially produced by the LS4P-I model ensemble mean, and 8 hotspot regions in the world were identified where June precipitation is significantly associated with anomalies of May TP land temperature. Consideration of the TP LST/SUBT effect has produced about 25–50% of observed precipitation anomalies in most hotspot regions. The multiple models have shown more consistency in the hotspot regions along the Tibetan Plateau-Rocky Mountain Circumglobal (TRC) wave train. The mechanisms for the LST/SUBT effect on the 2003 drought over the southern part of the Yangtze River Basin are discussed. For comparison, the global SST effect has also been tested and 6 regions with significant SST effects were identified in the 2003 case, explaining about 25–50% of precipitation anomalies over most of these regions. This study suggests that the TP LST/SUBT effect is a first-order source of S2S precipitation predictability, and hence it is comparable to that of the SST effect. With the completion of the LS4P-I, the LS4P-II has been launched and the LS4P-II protocol is briefly presented.

1 Introduction

Despite impressive progress in weather forecasting during recent decades (Bauer et al. 2015), subseasonal-to-seasonal (S2S) precipitation prediction in late spring and summer months, which contains a significant amount of extreme hydroclimate events such as droughts and floods, has remained poor to date. Supported by expanded predictive capabilities, a joint S2S Prediction Project of the World Climate Research Programme (WCRP) and the World Weather Research Programme (WWRP) of the World Meteorological Organization (WMO) has been tackling the so-called

---

Extended author information available on the last page of the article

weather–climate prediction desert ranging from 2 weeks to 3 months, "aiming to underpin new WMO operations on those time scales" (Vitart et al. 2017; Robertson et al. 2018; Merryfield et al. 2020). The activities include "understanding and adequately representing in model's processes that give rise to predictability in the Earth system", and "correcting for and reducing imperfections in models that may systematically degrade forecast quality" (Merryfield et al. 2020). In terms of the S2S predictability, the organization of tropical convection by the Madden–Julian oscillation (MJO) has been considered as a major source (Vitart et al. 2017; Woolnough 2019). Atmosphere–ocean interactions have also long been recognized as providing predictive value at different scales. For example, information on tropical sea surface temperature (SST) anomalies associated with the El Niño–Southern Oscillation (ENSO) have improved S2S prediction skill for precipitation and temperature over certain land areas including the contiguous United States (Hudson et al. 2011; Li and Robertson 2015; DelSole et al. 2017; Mariotti et al. 2018). Extratropical SST anomalies, such as in the midlatitude North Pacific, can also impact rainfall S2S prediction skill (McKinnon et al. 2016; Xue et al. 2012, 2016b, 2018; Diallo et al. 2019). However, studies have consistently shown that the SST only partially explains predictability (Mo et al. 2009; Scaife et al. 2009; Rui and Wang 2011; Pu et al. 2016; Xue et al. 2016a, b; Orth and Seneviratne 2017).

The land's role in the climate system at various spatial and temporal scales has been the subject of much research since the 1970s. The effects/mechanisms of a number of attributes of the land surface, such as albedo, soil moisture, vegetation, and snow, in land–atmosphere interactions have been extensively investigated (Charney et al. 1977; Shukla and Mintz 1982; Sud et al. 1988; Yasunari et al. 1991; Zeng et al. 1999; Koster et al. 2004; Xue et al. 2004, 2010; Seneviratne et al. 2010; Materia et al. 2022). The lack of observational data has presented a crucial limitation to progress. Land–atmosphere interaction studies have largely focused on the local feedbacks between land and atmosphere. However, how the land surface process can be applied for better S2S prediction of precipitation anomalies, especially droughts and floods, has not been highlighted in most previous land/atmosphere interaction studies.

It is only recently that the role of land surface processes in S2S predictability has been investigated. Studies using one Earth System Model (ESM) have shown that cold/warm spring land surface temperature (LST) and subsurface temperature (SUBT) in the Tibetan Plateau (TP) and Rocky Mountain areas would cause drought/flood in respective downstream regions (Xue et al. 2012, 2016b, 2018). Inspired by these results, the Global Energy and Water Exchanges (GEWEX) program launched in 2018 the initiative, "Impact of Initialized Land Temperature and Snowpack on Sub-seasonal to Seasonal Prediction" (LS4P, https://ls4p.geog.ucla.edu; Xue et al. 2019a, b, 2021). This community effort aimed to assess the impact of initializing LST and SUBT in high mountain regions on S2S prediction with multi-ESMs. Climate scientists, especially climate modelers, from more than 40 institutions worldwide, including major climate research and prediction centers, participated in the project.

The WCRP and WWRP joint S2S project has listed the study of land initialization and configuration as one of their major activities (Merryfield et al. 2020). The first LS4P paper (Xue et al. 2021) presented the LS4P objectives, the methodology to improve the LST/SUBT initialization in high mountain areas, and the first-phase experimental protocol (LS4P-I). The LS4P-I experiments focused on the remote effect of the LST/SUBT in the TP. This region was selected for several reasons: (1) the high elevation, (2) large geographical coverage, (3) special geographical location, (4) much stronger downward shortwave radiation than other areas resulting in very strong diurnal and seasonal changes of the surface energy components and other meteorological variables, such as surface temperature and the convective atmospheric boundary layer (Xue et al. 2017), and (5) availability of comprehensive and long-term near surface, subsurface, and planetary boundary layer measurements. The year 2003 was selected as a case study because an extreme summer drought/flood occurred to the south/north of the Yangtze River, respectively (Fig. 1a), after a very cold spring in the TP (Fig. 1c). The causes of the severe drought in the southern part of the Yangtze River Basin (SYRB) have not yet been identified. As such, the LS4P complements but is different from other international projects that focus on operational S2S prediction (Kirtman et al. 2014; Pegion et al. 2019).

The highlights of the LS4P-I results were presented in Xue et al. (2022). This paper elucidated new developments in the S2S prediction and provided a new and potentially far-reaching perspective to spark the community's interest in further exploration of the new approaches. The present paper is a follow-up of Xue et al. (2022) and aims to comprehensively analyze the LS4P Phase I results and assess its effects on S2S precipitation prediction. The TP LST/SUBT's effect is also compared with the SST effect here. Section 2 gives general background for the development of increased understanding of the LST/SUBT effect in the S2S prediction. Sections 3 and 4 present preliminary assessments of the LS4P-I ESMs' performance in the 2003 summer case and the LS4P Phase I's experimental design, as well as assess the effect of the TP LST/SUBT anomaly on the global S2S precipitation prediction, respectively. Section 5 explores the relevant mechanism with a main focus on how the TP LST/SUBT affects the East Asian summer monsoon. The mechanism at work for the TP LST/SUBT's effect on the
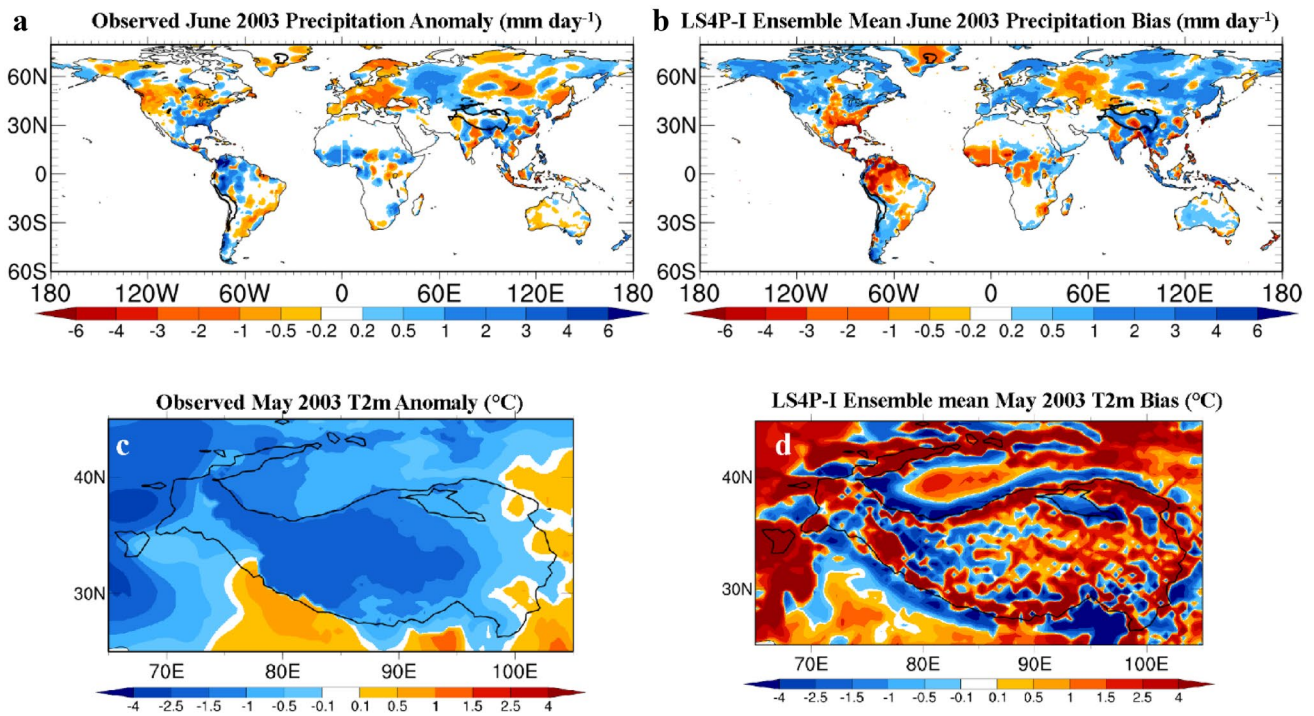
Fig. 1 **a** Observed precipitation anomalies (mm day^{-1}) for June 2003. **b** As in **a** except for LS4P-I multi-model ensemble simulation biases. **c** As in **a** except for T2m (°C) for May 2003. **d** As in **b**, except for T2m (°C) for May 2003

global atmospheric circulation through teleconnection will be discussed in a separate paper. Section 6 compares the LST/SUBT and SST effects. Section 7 provides the summary along with further discussion.

2 Background: evidence of land memory and its effect on prediction

It is well known that skillful forecasting more than 30 days ahead requires information on the slow-varying components of the climate system, of which the SSTs are a prime example. The ocean surface conditions with low frequency variability interact with the atmosphere to affect the variability and development of the atmospheric circulation with some degree of predictability (Mariotti et al. 2018). The land memory effect due to land temperature on S2S prediction, however, has long been overlooked. Questions have been raised regarding whether land surface temperature anomalies that interact with the atmosphere can be sustained for several weeks to months to provide a stable boundary forcing that could enhance the S2S predictability. That said, demonstrating the existence of land memory from observations is the key aspect in support of applying the land temperature memory for S2S prediction studies.

In most parts of the world, large-scale soil layer measurements only reach 50 cm below the surface, which is not

sufficient to provide comprehensive information on land memory. Fortunately, decadal field measurements by the Third Pole Environment (Ma et al. 2008; Li et al. 2020), the Tibetan Plateau Atmospheric Scientific Experiment (TIPEX, Xu et al., 2008; Zhao et al. 2018) and other related projects have made available large-scale surface plus subsurface data at deeper levels. Based on the observed data of the China Meteorological Administration (CMA, https://data.cma.cn, Zhao et al. 2007) from 80 ground stations over the TP, of which 14 have soil temperature measurements to a depth of 320 cm covering the period from 1981 to 2005, it has been found (Liu et al. 2020a, b) that in the TP anomalies in 2-m air temperature above the land surface (T2m), LST, SUBT, snow, and surface albedo exhibit long persistence. Anomalies in LST are highly correlated to those in snow, surface albedo, and SUBT in current and preceding months. Anomalies in surface albedo and SUBT have a memory of 1–3 months. The duration of the anomalies is significantly longer in winter and spring than in other seasons (see Figures 1 and 2 in Liu et al. 2020a). Meanwhile, based on observed T2m data during the period 1981–2010 from CMA and Climate Anomaly Monitory System (CAMS, Fan and Van den Dool 2008), analyses show that the T2m anomaly in the TP and the Western U.S., mainly over the Rocky Mountain area, could persist for several months, especially during boreal spring (see Figure 1 in Xue et al. 2021). As such, there is a potential for the LST/SUBT to provide land

memory at the S2S time scale. In the following, all seasons refer to the Northern Hemisphere.

Maximum covariance analysis (Von Storch and Zwiers 1999; Xue et al. 2018) using observed T2m and precipitation data has been carried out to explore the relationship between spring T2m anomalies in high mountain regions, mainly in the TP and the Rocky Mountains, and summer precipitation in their respective downstream regions. The results showed a significant correlation between these two variables and revealed possible non-local effects of large-scale spring T2m and LST/SUBT anomalies over high mountains in geographical regions, upstream of areas that experience late spring or summer drought/flood. Specifically, warm/cold spring in the TP or the Western U.S. contributes to downstream late spring–summer flood/drought. Such a statistical lag relationship has been further confirmed as representing a causal relationship by one ESM and one regional climate model (RCM) in a series of prototype studies with drought/flood scenarios in various regions over different years (Xue et al. 2012, 2016a, b, 2018; Diallo et al. 2019). For example, for the May 2015 flooding in the Southern Great Plains and June 2003 drought in the SYRB, the May LST/SUBT anomalies in the Rocky Mountains and the TP produced 29% and 34% of the rainfall anomalies, respectively, while the SST effect produced 34% and 38% of rainfall anomalies, respectively.

Moreover, statistical analyses and regression testing based on observational data have revealed that the significant lag relationship between May T2m anomaly over the TP and June precipitation anomaly downstream not only exists over East Asia, but also over many parts of the world (Figures 1 and S2 in Xue et al. 2022). Figure 1 in Xue et al. (2022) shows the observed June precipitation difference between the 5 coldest and 5 warmest Mays in the TP during the period 1981–2015. These years were selected based on the Tibetan Plateau Index (TPI, Xue et al. 2022) which is defined as the averaged T2m anomaly over the region bounded by 29° N–37° N and 86° E–98° E. The figure shows that, in addition to the statistically significant dry SYRB, there was a dipole anomaly in North America, mainly over the Great Plains. Meanwhile, significant June precipitation anomalies are evident in other regions, such as northern South America, the Sahel region, Indonesia, Western and Northern Europe, etc. Further study indicates that such an influence is underscored by Tibetan Plateau-Rocky Mountain Circumglobal (TRC) wave train. The present paper uses multiple ESMs to examine whether such lag relationships indeed suggest a causality.

Furthermore, in recent years, additional modeling studies with ESMs and RCMs as well as data analyses have investigated the linkage between S2S predictability and LST/SUBT effect (Yang et al. 2019, 2021, 2022; Shukla et al. 2019; Diallo et al. 2022; Qi et al. 2022; Qiu, et al. 2022; Sugimoto et al. 2022; Xu et al. 2022; Saha et al. 2023), some of which

are published in this special issue. The prelude of this special issue presents a brief overview of these results. The presents paper mainly concentrates on the LS4P-I ensemble mean results.

3 Preliminary assessment and experimental design

3.1 Preliminary assessment of control experiment

As discussed in the Introduction, the initial LS4P-I goal was to assess whether the results produced by one ESM (Xue et al. 2018) could be reproduced by other ESMs, with a focus on the remote effect of the TP on S2S precipitation predictability over East Asia. The time period selected for the LS4P-I was May–June 2003. The summer of 2003 was characterized by a severe drought over the SYRB, with an average anomalous precipitation rate of -1.40 mm day^{-1} within 112–121° E and 24–30° N. To the north of the Yangtze River basin, there was above-normal precipitation causing pluvial flooding, with anomaly rates of 1.32 mm day^{-1} over the area within 112–121° E and 30–36° N (Fig. 1a). In 2003, the observations show a cold spring over the TP, during which the T2m in May above 4000 m was 1.40 °C below the climatological average (Fig. 1c). In this study, we use the Climate Research Unit (CRU, Harris et al. 2014) data for precipitation, and CMA data (Han et al. 2019) within China, while CAMS data (Fan and Van den Dool 2008) were used elsewhere for the T2m.

In addition to East Asia, Fig. 1a shows substantial positive and negative precipitation anomalies over many parts of the world. It should be pointed out that in many of these regions, such as the Great Plains in North America, Sahel in West Africa, Indonesia, India, Japan, and Europe, the precipitation anomaly patterns in Fig. 1a also appeared in other years with observed cold Mays as shown in Figure 1 of Xue et al. (2022). The present paper will address whether the observed precipitation anomalies over many parts of the world, as shown in Fig. 1a, are associated with the TP cold spring T2m anomaly using multiple ESMs. To the authors' knowledge, this has not been a subject of any previous studies.

The LS4P-I designed a series of experiments to address the impact of a large-scale LST/SUBT anomaly in the TP in climate models on S2S predictability and to compare this effect with the ocean state in S2S predictions. A comprehensive discussion on the LS4P-I experimental designs is presented in Xue et al. (2021). The first experiment of the LS4P-I, referred to as Exp-CTRL (Table 1), aimed to evaluate whether the current state-of-the-art ESMs can reproduce the observed May 2003 T2m anomaly over the TP as well as summer drought/pluvial flood conditions over East

Table 1 Summary of different experiments under the LS4P-I framework

Experiment name	LST/SUBT initialization (imposing mask)	SST	Note
Exp-CTRL	No	May–June 2003 SST	Default run from the Earth System Model with starting date around late April 2003 to 30 June 2003
Exp-LST/SUBT	Yes	May–June 2003 SST	Same as Exp-CTRL, but with the mask imposed over the Tibetan Plateau at the 1st time-step of the ESM integration
Exp-SST	No	May–June Climatological SST (1981–2010 mean)	Same as Exp-CTRL, but with the 2003 SST replaced by the climatological SST

HR high resolution, *LR* low resolution

Asia. The goal of this baseline experiment was to determine whether we need to improve the LST/SUBT initialization over the TP for better S2S prediction. The results from 16 ESMs (Table 2)[1] that completed the LS4P-I's major experiments are presented in this paper. Each ESM conducted an approximately 2-month long simulation from late April through June 2003 with their normal setting for a S2S prediction of atmospheric and land initial conditions and ocean surface boundary conditions. Except for the CNRM-CM6-I-CMIP (hereafter referred to as CNRM CMIP) and the ECMWF-IFS, every ESM used daily reanalysis data to specify May and June 2003 SST and sea ice conditions. The CNRM-CMIP and the ECMWF-IFS specified ocean initial conditions at the beginning of the integration and ran the model in a fully coupled land–atmosphere–ocean configuration. The LS4P-I protocol required at least six ensemble members, but most groups provided more than 10 ensemble members (Table 2).

In general, the current state-of-the-art LS4P-I ESMs can produce reasonable global scale climate features. Figure S1 in the supplement displays the spatial distribution of global June precipitation from each ESM, the ESM ensemble mean, and the observation. Major features in the global spatial distribution of June 2003 precipitation are well simulated, such as the Intertropical Convergence Zone (ITCZ), the northern summer monsoons, the second rainfall maximum in mid-latitudes, etc. Table 3 lists the statistics for bias, root-mean-squared error (RMSE), and global spatial correlation coefficients with June 2003 precipitation observations for each model and the ensemble mean. At the global scale, the spatial correlations, bias, and RMSE of most ESMs range between 0.7–0.8, −0.2 to 0.4 mm day^{-1}, and 1.7–2.4 mm day^{-1}, respectively. The spatial correlations

are particularly high for every model, which is consistent with the spatial patterns displayed in Fig. S1. The ensemble mean has the lowest RMSE: 1.6 mm day^{-1}. Due to the limited scope of this paper, the following discussion will focus on the ensemble mean. A future paper will be dedicated to discussing characteristics of responses and spread of the ESM ensemble members to the LST/SUBT initialization.

At the regional scale, however, several model errors are apparent. None of the LS4P-I ESMs can produce observed May 2003 TP T2m cold anomaly properly: most of the models have large biases (Table 3). For example, there are 12 LS4P-I ESMs with a warm bias over the TP ranging from about 0.38 to 2.86 °C with a mean bias of +1.54 °C and remaining models with a cold bias ranging from about −0.35 °C to −2.35 °C with a mean bias of −1.07 °C. For comparison, the observed T2m inter-annual standard deviation over the TP is only about 0.7 °C. Because the warm biases are dominant among the LS4P-I models, the ensemble mean also displayed a strong warm bias (Fig. 1d), +1.02 °C. Furthermore, the LS4P-I ESMs produce large biases for June precipitation not only over East Asia but over many other parts of the world (Fig. 1b, Table 3). For instance, for the SYRB, the ensemble mean shows a wet bias of 1.10 mm day^{-1} versus the observed drought of −1.39 mm day^{-1}. Most models produce large wet biases. Only a few models have a small bias but with a large RMSE, suggesting the small mean biases are just the artifact of the cancellation between positive and negative biases in the region. In addition, Table 3 lists large errors in the simulation over the Southern Great Plains, which will be further discussed later.

A comparison of Fig. 1a, b reveals consistent spatial patterns with opposite signs over many parts of the world, such as North America, northern South America, the Sahel, the Eurasian continent, etc. The ensemble mean has a negative bias in the regions with an observed positive anomaly and vice versa. The global spatial correlation coefficient between Fig. 1a, b is −0.55. According to Fig. 1c, d, the May TP observed anomaly and model bias also show generally

___

[1] The LS4P-I has a total of 18 ESM simulations as shown in Table 2. However, we received the last two ESM (CIESM, BESM) results after we have completed all of the analyses. Thus, their results will not be presented in the ensemble means as discussed throughout the paper.

Table 2 List of LS4P-I models in this study with relevant information

LS4P-I models	Institution name	Resolution	Exp-CTL	Exp-LST/SUBT	Exp-SST	Ensemble size	Short name	Key references*
ACCESS-S2	Bureau of Meteorology, Australia	N216L85, ocean 0.25	Yes	Yes	No	11 members	ACCESS-S2	MacLachlan et al. (2015)
AFES-HU ver 4.1	Hokkaido University, Japan	T79 (~150 km), and 56 vertical level up to about 0.1 hPa	Yes	Yes	Yes	30 members	AFES-HU	Nakamura et al. (2015)
BESM**	National Institute for Space Research, Brazil	T062L42	Yes	Yes	No	10 members	BESM	Nobre et al. (2013)
CAS-ESM	Institute of Atmospheric Physics, Chinese Academy of Sciences, China	1.4°×1.4°	Yes	Yes	Yes	8 members	CAS-ESM	Lin et al. (2016)
CAS-FGOALS-f2	BNU and IAP/LASG, China	100 km×100 km	Yes	Yes	Yes	8 member	FGOALS-f2	Bao et al. (2019)
CFS UCLA (CFS/SSiB2)	University of California—Los Angeles, USA	T126 (~1°×1°) and 47 vertical levels	Yes	Yes	Yes	10 members	CFS/SSiB2	Xue et al. (2004); Lee et al. (2019)
CIESM**	Tsinghua University, China	~1-degree	Yes	Yes	Yes	8 members	CIESM	Lin et al. (2019, 2020)
CMCC-SPS3	Fondazione Centro euro-Mediterraneo sui Cambiamenti Climatici (CMCC), Italy	ne30np4 (~111 km grid spacing at the equator) and 46 atmospheric vertical levels up to 0.2 hPa	Yes	Yes	Yes	20 members	CMCC-SPS3	Samna et al. (2016)
CNRM-CM6-1 AMIP	CNRM, France	T1127 (~150 km), and 91 levels up to 0.01 hPa	Yes	Yes	Yes	30 members	CNRM AMIP	Voldoire et al. (2019)
CNRM-CM6-1 CMIP	CNRM, France	Atmos: same as CNRM-CM6-1 AMIP Ocean: ORCA1 (~100 km), 75 vertical levels	Yes	Yes	No	30 members	CNRM CMIP	Voldoire et al. (2019)
ECMWF-IFS	ECMWF, United Kingdom	Atmos: Tco199 (~25 km), 91 vertical Levels Ocean: ORCA025 (~25 km), 75 vertical levels	Yes	Yes	Yes	30 members	ECMWF	Johnson et al. (2019)
E3SM	Lawrence Livermore National Laboratory, USA	1°×1° and 72 levels up to ~0.1 hPa	Yes	Yes	Yes	6 members	E3SM	Golaz et al. (2019); Tang et al. (2019)
GRAPES GFS	China Meteorological Administration, China	0.5°×0.5°	Yes	Yes	No	8 members	GRAPES	Chen et al. (2020)
IITM CFS	Indian Institute of Tropical Meteorology, Ministry of Earth Sciences, India	T126 (~1°×1°) and 47 levels, up to 0.01 hPa	Yes	Yes	Yes	10 members	IITM CFS	Saha et al. (2017)
JMA/MRI-CPS2	Japan Meteorological Agency/Meteorological Research Institute, Japan	Atmosphere: 110 km Ocean: 1°×0.3–0.5°	Yes	Yes	Yes	10 members	JMA CPS2	Takaya et al. (2018)

Table 2 (continued)

LS4P-I models	Institution name	Resolution	Exp-CTL	Exp-LST/SUBT	Exp-SST	Ensemble size	Short name	Key references*
KIM HR	Korea Institute of Atmospheric Prediction Systems, South Korea	T254L64 (~ 55 km; up to 0.3 hPa)	Yes	Yes	Yes	10 members	KIM HR	Hong et al. (2018) but with spectral dynamical core (Hong et al. 2013)
KIM LR	Korea Institute of Atmospheric Prediction Systems, South Korea	T126L42 (~ 111 km; up to 2.5 hPa)	Yes	Yes	Yes	10 members	KIM LR	Hong et al. (2018) but with spectral dynamical core (Hong et al. 2013)
NASA GEOS5	NASA Goddard Space Flight Center, USA	1-degree	Yes	Yes	Yes	30 members	NASA GEOS5	Molodet al. (2020)

*References are listed in the Supplemental

**The models' results are not used in the paper due to late submission

opposite signs. As discussed earlier, the analyses based on observational data suggest a lag relationship between the May T2m anomaly over the TP and the June precipitation anomaly over many parts of the world, many of which are coincident with the areas with large bias and large anomalies as shown in Fig. 1. The observed lag relationship between May T2m over the TP and June precipitation in many areas over the world and the models' T2m bias over the TP and precipitation biases over many parts of the world that were noticed during the LS4P-I activity have provided a strong motivation for evaluating the LS4P-I results beyond East Asia to a much larger spatial scale.

3.2 Experimental design

The LS4P hypothesis is that if the May land temperature anomaly in the TP contributes to the June precipitation anomaly, then by reducing the May land temperature bias in the TP through initialization, the ESMs should produce better prediction of the June precipitation anomaly. To test the LS4P hypothesis, the second experiment, referred to as Exp-LST/SUBT, was designed to reduce the ESMs' May TP T2m bias in order to generate the observed cold TP spring anomaly, then to examine its impact on June precipitation. An innovative approach for initializing the TP LST/SUBT to produce an adequate May TP T2m anomaly was developed, which is comprehensively discussed in Xue et al. (2021). Note that LST and SUBT are prognostic variables which need to be initialized in a model simulation, while T2m is a diagnostic variable with no need for initialization. However, we use the observed T2m as a proxy for initializing LST and SUBT because T2m and LST are very close in magnitude and variability, and LST and SUBT are highly correlated. Moreover, the memory in the soil subsurface is one of the major sources for producing surface temperature anomalies (Liu et al. 2020a). As such, if the deep soil is not initialized, the imposed initial soil surface temperature anomaly and corresponding T2m anomaly would disappear after a couple of days of model integration.

The new surface temperature initialization proposed by the LS4P remedies the inability of the LS4P global models to realistically generate observed May 2003 TP T2m anomalies. Our preliminary research suggests that adjusting both LST and SUBT initial conditions based on the observed T2m anomaly and model bias is an efficient way for the LS4P ESMs to produce the observed May monthly mean T2m anomalies. In Exp-LST/SUBT, the model simulations were conducted using the new LST/SUBT initial condition over the TP, with all of the other initial and boundary conditions identical to Exp-CTRL. As such, the differences between Exp-LST/SUBT and Exp-CTRL show the effect of the LST/SUBT initialization and the influence of a different

Table 3 Mean bias, root-mean-square error (RMSE), and spatial correlation (SC) of May 2003 T2m and June 2003 precipitation in Exp-CTRL relative to observation

	Precipitation (mm day^{-1})							T2m (°C)		
	Global			South of Yangtze River Basin		Southern Great Plains		Tibetan Plateau above 4000 m		
	Bias	SC	RMSE	Bias	RMSE	Bias	RMSE	Bias	SC	RMSE
ACCESS-S2	0.33	0.79	2.01	0.83	2.63	−1.87	2.40	1.30	0.60	3.61
AFES-HU	0.43	0.68	2.32	−1.67	3.11	−0.34	1.58	−0.53	0.39	5.08
CAS-ESM	−0.03	0.73	2.16	0.12	2.87	−1.59	2.41	0.59	0.51	3.93
FGOALS-f2	−0.59	0.67	2.45	−0.69	3.01	−2.83	3.19	0.95	0.51	3.77
CFS/SSiB2	0.36	0.72	2.28	1.59	3.98	−2.05	2.40	2.15	0.48	3.98
CMCC-SPS3	0.14	0.77	2.06	1.35	2.73	−1.45	2.06	2.64	0.51	4.48
CNRM-CMIP*	0.12	0.76	2.15	2.35	4.70	−2.18	2.43	−0.35	0.53	4.20
ECMWF	0.11	0.85	1.65	1.59	2.71	−1.91	2.32	−2.35	0.61	4.21
E3SM	0.14	0.78	2.01	0.95	2.47	0.60	1.95	0.42	0.50	4.01
GRAPES	−0.09	0.61	2.17	2.35	4.57	−2.30	2.76	0.38	0.54	3.26
IITM CFS	0.03	0.71	2.22	−0.58	3.30	−1.45	2.12	1.95	0.55	3.98
JMA CPS2	0.10	0.78	1.93	−0.22	2.77	−0.89	1.81	1.38	0.46	4.47
KIM HR	−0.18	0.67	2.34	2.92	5.00	−3.05	3.47	2.86	0.43	5.80
KIM LR	−0.24	0.76	2.03	2.49	4.30	−2.50	2.95	1.64	0.43	5.47
NASA GEOS5	0.42	0.81	2.07	1.86	3.09	−1.90	2.41	2.27	0.52	3.96
Ensemble Mean	0.13	0.78	1.59	1.10	2.84	−1.67	2.17	1.02	0.50	4.30

*CNRM has two runs as shown in Table 2. However, there is only one control simulation

TP surface temperature (with/without LST/SUBT initialization) on prediction.

However, as discussed earlier, the LS4P models have either warm (12 models) or cold (4 models[2]) biases. The LST/SUBT initialization procedure for models with warm/cold biases is delineated in the red/blue box, respectively, shown in the schematic diagram presented in Fig. 2. The 'mask' for each model was calculated using the spatial patterns of the climate anomaly and the model bias over the plateau. The basic concept of the mask is shown in Fig. 2. Further details of the mask determination can be found in Eq. (1) and in Figures 2 and 3 in Xue et al. (2021). The mask was 'imposed' on both the LST and SUBT at the first time-step of the Exp-LST/SUBT. Figure 2 demonstrates that for ESMs with warm/cold bias, the initialization would make the initial LST and SUBT cooler/warmer in Exp-LST/SUBT, respectively, to reduce the model bias. After these masks have been imposed on all of the LS4P-I models, we obtain a set of model ensembles having reasonable observed T2m anomaly on average.

The primary LS4P-I objective was to examine whether the observed *cold* May 2003 TP causes the observed June precipitation anomalies. For this purpose, we defined the experimental run with a cold/warm initial condition over the TP as the cold case/warm case, respectively, regardless of whether the run belongs to Exp-CTRL or Exp-LST/SUBT

or whether the model has a warm or cold bias (Fig. 2). The differences between the 16 ESM ensemble means of the cold cases and warm cases are used in the following discussion to examine the simulated effect of cold May TP LST/SUBT on the June 2003 precipitation and other fields.

Exp-SST tests the SST effect on the June 2003 precipitation (Table 1). There were two approaches for this test. For most modeling groups, in Exp-SST, the specified 2003 daily SST conditions were replaced by the climatological daily SST. For CNRM CMIP, the 2003 initial condition used in Exp-CTRL was replaced by the climatological initial condition. Therefore, the difference between Exp-CNTL and Exp-SST represents the effect of the 2003 SST anomaly on precipitation. The year 2003 was an ENSO year. The CNRM CMIP checked their models' SST simulations to be sure that their models produced realistic SST conditions along the western coast of South America and eastern Pacific. SST conditions in these regions are difficult to simulate (Mechoso et al. 1995). The precipitation difference between the Exp-CTRL (with the 2003 ocean state) and the Exp-SST run (with the climatological ocean state) are compared with the observed anomaly in 2003 to assess the global ocean state effect on precipitation, then it is compared with the LST/SUBT effect from the Exp-LST/SUBT results. These three experiments are listed in Table 1.

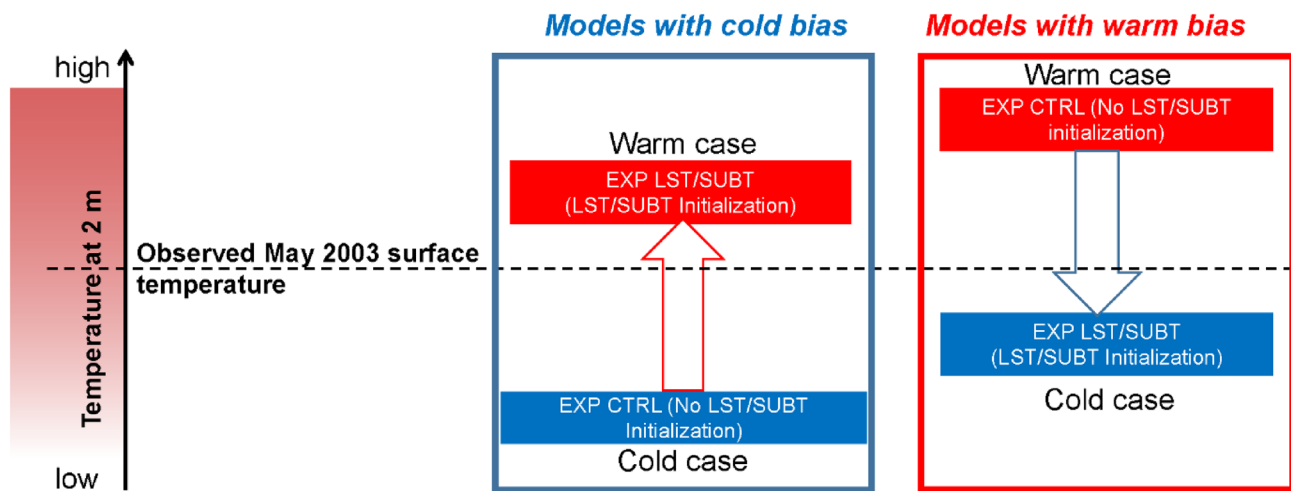[2] CNRM-CMIP and CNRM-AMIP have the same EXP-CTRL.

Fig. 2 Schematic diagram of model initialization using masks for models with cold/warm biases over the Tibetan Plateau. Notes: (1) The LST/SUBT initialization procedure in Exp-LST/SUBT for models with warm/cold biases are delineated in the red/blue box, respectively. (2) Exp-CTRL (or control run) has no LST/SUBT initialization; Exp-LST/SUBT (or sensitivity run) is similar to Exp-CTRL, except that an LST/SUBT initialization was used in the first time-step using a mask over the Tibetan Plateau to minimize the model bias. (3) We refer to the runs with a cold/warm Tibetan Plateau initial condition as the cold case/warm case, respectively, regardless of whether the model runs originally were from Exp-CTRL or Exp-LST/SUBT
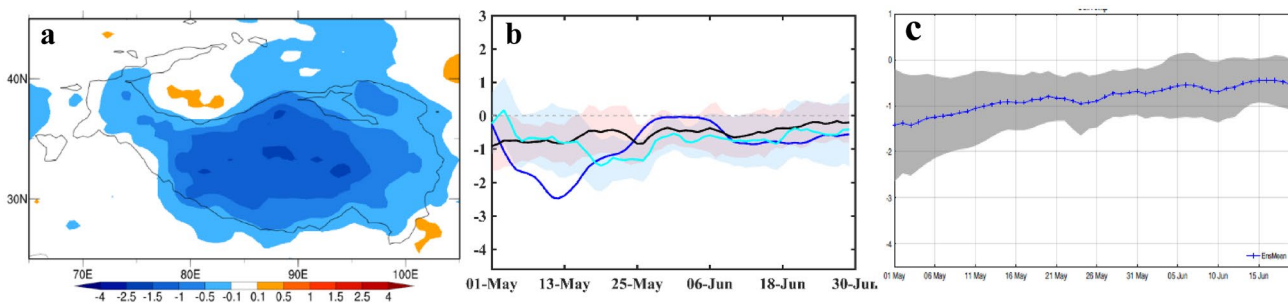
Fig. 3 Simulated differences between cold cases and warm cases. **a** Ensemble mean T2m difference on May 1st over the TP; **b** Time series of TP T2m difference from the ensemble mean (black line), observed 2003 T2m anomaly (blue line), and observed anomaly of 8 cold years mean (dark cyan line); **c** Time series of TP soil surface temperature from ensemble mean over the TP. Notes: (1) The light red shading in **b** and dark shading in **c** show the standard deviation between ensemble members, and the light cyan shading shows the standard deviation in 8 cold years. (2) The selection of 8 cold Mays in **b** is based on half standard deviation of the observational data during 1991–2015 when the daily data are available

4 TP LST/SUBT effect

4.1 TP T2m simulation

To assess the effect of spring TP LST/SUBT on the S2S precipitation prediction using the ESM, the first step is to reproduce the observed May 2003 TP T2m anomaly that affects the exchange of heat and momentum fluxes between the TP surface and atmosphere. Because current ESMs used within LS4P have deficiencies in adequately producing the TP T2m anomaly as discussed in Sect. 3.1, an initialization method has been developed to overcome this shortcoming.

This new land temperature initialization approach imposes a temperature mask (ΔT) on every grid point over the TP based on the observed T2m anomaly and model's bias over the region (Xue et al. 2021). This section examines the effect of this T2m initialization.

Figure 3 shows that after imposing the LST/SUBT mask over the TP at the 1st time step of the model integration, the ensemble mean difference between the cold and warm cases has produced a cold TP in May and June, but not as cold as the observed anomaly, especially in May. To exhibit the effect of the mask on the T2m simulation, we display its values over the TP on May 1st in Fig. 3a. The LS4P-I models have various starting dates and different ensemble members,

Table 4 Observed/simulated May 2003 T2m and June 2003 precipitation anomalies/differences due to LST/ SUBT effects

	May 2003 T2m (°C)		June 2003 precipitation (mm day^{-1})			
	TP above 4000 m		South of Yangtze River Basin		Southern Great Plains	
	Obs. anomaly/simulated difference	% of Obs.	Obs. anomaly/simulated difference	% of Obs.	Obs. anomaly/simulated difference	% of Obs.
Observation	− 1.40	100	− 1.39	100	0.87	100
ACCESS-S2	− 0.85	60.71	− 0.76	54.68	0.11	12.64
AFES-HU	− 1.13	80.71	0.09	− 6.47	0.01	1.15
CAS-ESM	− 0.57	40.71	− 0.22	15.82	0.34	39.08
FGOALS-f2	− 1.49	106.42	0.12	− 8.63	0.59	67.82
CFS/SSiB2	− 1.46	104.28	− 1.32	94.97	0.60	69.00
CMCC-SPS3	− 0.39	27.86	0.54	− 38.85	0.39	44.83
CNRMAMIP	− 0.96	68.57	− 0.86	61.90	− 0.04	− 4.60
CNRMCMIP	− 1.07	76.43	− 1.45	104.32	− 0.05	− 5.75
ECMWF	− 0.35	25.71	− 0.37	26.62	0.74	85.06
E3SM	− 0.84	60.00	− 2.36	169.78	1.01	116.01
GRAPES	− 1.11	78.28	− 0.31	22.30	1.76	202.30
IITMCFS	− 0.25	17.86	0.20	− 14.39	0.46	52.87
JMA CPS2	− 0.99	70.71	− 0.61	43.88	− 0.04	− 4.60
KIM HR	− 0.12	8.60	− 0.65	46.76	0.68	78.16
KIM LR	− 0.50	35.71	− 0.84	60.43	− 0.36	− 41.38
NASAGEOS5	− 1.00	71.43	− 0.43	31.00	− 0.13	− 14.94
Ensemble mean	− 0.82	58.57	− 0.58	41.73	0.38	43.68

each of which may also have different starting times. May 1st is the first day of the model's May–June integration required in the experimental design; therefore, every run contains this date in their model outputs; this date is also close to the dates when the initial LST/SUBT mask was imposed. Figure 3a shows that by May 1st, the ensemble mean has a cold T2m spatial distribution over the TP of about − 1 °C on average, which is comparable to but not as cold as the observed May TP anomaly of − 1.4 °C. We will discuss this issue further in the next paragraph and in Sect. 7. Figure 3b displays the daily time series of the 15-day running mean difference of the T2m ensemble means between the cold and warm cases. For comparison, the observed 15-day running mean of daily May 2003 T2m anomaly is also displayed in the figure. The results in Fig. 3b show that the ensemble mean difference produces a persistent cold anomaly during May: the daily T2m difference starts from about − 1.0 °C on May 1st and is about − 0.5 °C by the end of May. On average, the ensemble mean produced − 0.82 °C difference over the TP (Table 4, Fig. 3b), which is about 60% of the observed May anomaly. The May T2m difference for each ESM's is listed in Table 4. Ten out of 16 models generated 60–100% of the observed anomaly.

The results discussed above revealed that the LS4P models are still unable to fully produce the observed anomalies after imposing the mask. Xue et al. (2021) has identified two possible reasons which cause this problem: (1) deficiencies

in land models, such as too shallow soil depths and/or simplified parameterizations for heat transfer in soil layers, and (2) large discrepancies between the initial atmospheric conditions from reanalysis data and observed anomalies of TP LST. As discussed in Xue et al. (2021), for weather forecast and S2S prediction, a "shock adjustment" methodology has been implemented in many prediction centers to avoid an inconsistency between the atmosphere, land, and ocean initial conditions due to their different sources, and the belief that the atmospheric component is considered to be relatively the most reliable. In the current study for LS4P-I, our intention is to initialize the LST/SUBT in order to influence the lower atmosphere since the corresponding initial condition from reanalysis also has inherent errors. Since our approach is still in the early development stage, before another type of "shock adjustment" is developed (using the land condition to adjust lower atmosphere), a number of modeling groups started the model simulation earlier, for instance, on 1 April, to have sufficient time for the lower atmosphere to spin up and to be consistent with the within-mask imposed soil surface conditions. Further improvement in LST initialization is necessary.

The May monthly mean differences in some models are not that high due to their weakness in preserving soil memory. Nevertheless, in the early part of May the models can produce suitable heating changes to perturb the atmospheric circulation. Such a situation also occurs during tropical

Fig. 4 Observed and simulated May T2m differences (°C). **a** Observed May T2m difference between 12 cold Mays and warm Mays, **b** May T2m ensemble mean difference due to LST/SUBT effects, and **c** same as **b** except for the SST effects. Note: There are 12 cold and 12 warm Mays selected during 1981–2015 based on monthly mean observational data

Observed May T2m difference between TP 12 cold and 12 warm TP Mays

May 2003 T2m Ensemble Mean difference due to the LST/SUBT effects

May 2003 T2m Ensemble Mean difference due to the SST effects
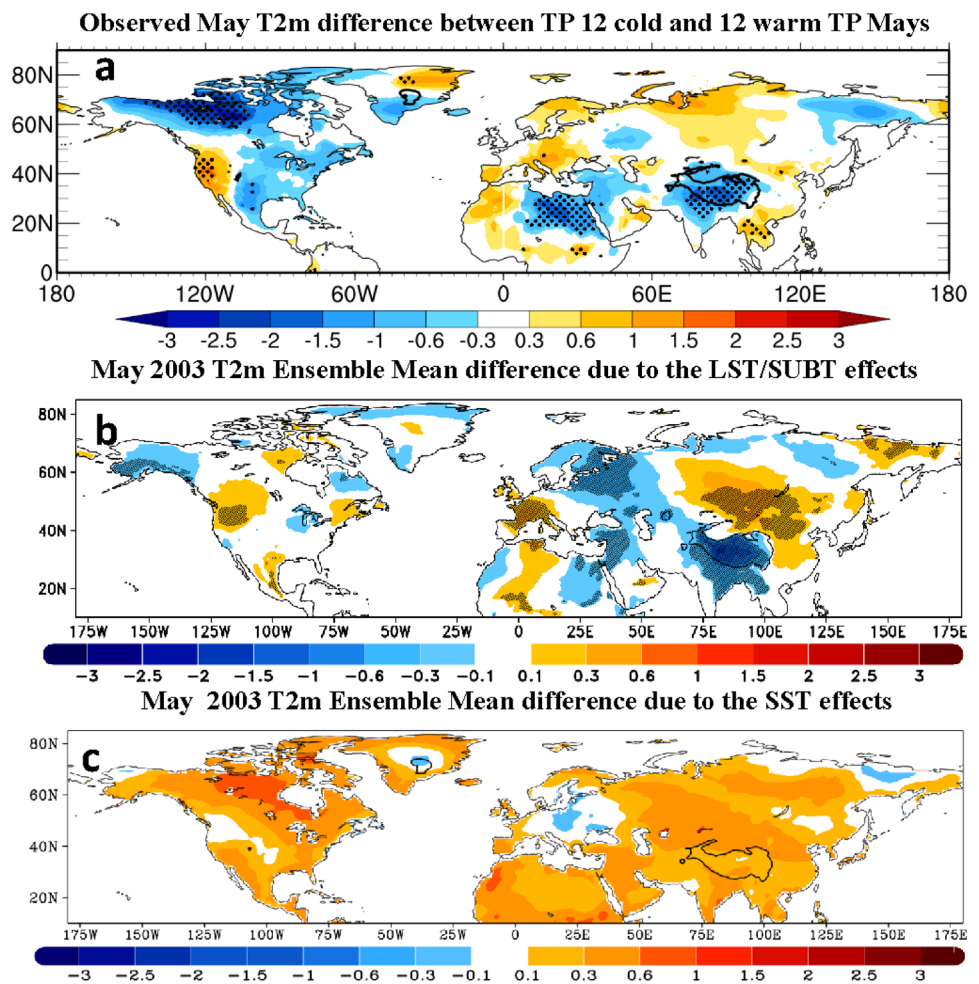
ocean heating events. An examination of the midlatitude response to localized equatorial ocean heating events that last for only a couple of days finds that upper-tropospheric structure of response to short pulses is remarkably similar to that to steady tropical heating (Branstator 2014).

The variability in the observation for May 2003 is larger than in the simulation (blue and black lines in Fig. 3b, respectively). The simulated TP T2m is not as cold as the observed during most of the period (Fig. 3b). The persistent and substantial cold anomaly, however, has been produced in the model simulation. The variability of the ensemble mean T2m difference seems to be more consistent with that of the simulated soil surface temperature (Fig. 3c), for which soil initial temperature condition was imposed and every model provides output for this soil layer. In addition to the similar variability between soil surface temperature and T2m, the TP soil temperature during May (Fig. 3c and Fig. S2) is colder than T2m (Figs. 3b and 4b). This feature suggests that soil temperature and memory likely contribute to the cold T2m. We further select 8 cold years from 1991 to 2015, which are 1992, 1993, 1997, 2001, 2002, 2003, 2005, and 2009, for analysis. The daily T2m data are available only

after 1990. The light red and cyan shadings in Fig. 3b represent the regions bounded by plus and minus the standard deviations from the ensemble members and 8-year observation, respectively. During most periods, the ESMs' standard deviations are generally within the ranges of that in observed cold TP years, suggesting that overall, the LS4P-I-produced T2m is consistent with observed cold May in the TP.

In principle, the T2m is more controlled by the local energy balance at the terrestrial surface, i.e., by the local difference between net radiation and heat fluxes. However, T2m anomalies over certain areas have been shown to have a possible relationship with the TP T2m anomaly. To explore the relationship between TP T2m and T2m in other parts of the world, Fig. 4a shows the T2m differences between 12 cold and 12 warm TP Mays from 1981–2015.[3] Figure 4b displays T2m differences in May 2003 between the ensemble means

---

[3] Warm Mays: 1981, 1984, 1989, 1991, 1994, 1995, 1996, 1998, 1999, 2000, 2007, 2008.
cold Mays: 1982, 1983, 1986, 1987, 1990, 1992, 1997, 2001, 2002, 2003, 2005, 2009. The daily data are available only after 1991.

of the cold and warm cases for that month. The anomaly patterns shown in Fig. 4a, b are generally similar, suggesting that the global spatial distribution of the simulated T2m anomaly in May 2003 is largely consistent with the Mays having a cold TP. The most outstanding common features in these two figures are the anomalies with opposite signs in the Western U.S., mainly over the Rocky Mountains. Because of the close relationship between the T2m in the TP and in the Rocky Mountains, we define a Rocky Mountain Index (RMI) as the averaged T2m observed anomaly averaged over the region bounded by 32° N–45° N and 110° W–125° W (Xue et al. 2022). A Tibetan Plateau-Rocky Mountain Circumglobal (TRC) wave train modulated by the TP land temperature perturbation from the TP through northeast Asia and the Bering Strait to the western part of North America has been identified (Figure 4b in Xue et al. 2022). The T2m anomaly patterns from the TP to the RMI area in Fig. 4a, b are generally consistent with the TRC wave train.

Figure 4a also exhibits a large negative anomaly in the Eastern U.S., which does not exist in Fig. 4b, suggesting that it is likely not associated with the TP T2m anomaly but probably with the anomaly in the Western U.S. Furthermore, both Fig. 4a, b show positive and negative anomalies in Southern Europe and central Europe/Middle East, respectively. It is still unclear at this stage whether these anomalies are associated with those in the TP. Further investigation is necessary to gain more insight on this result.

4.2 TP LST/SUBT effects on precipitation

The important role of the TP in determining the large-scale features of the atmospheric circulation has long been recognized. The view that the TP's thermal, dynamic, and mechanical forcing drives the Asian monsoon has been widely reported in the literature. In addition to the TP's topographic effect, studies based on observations and modeling have indicated that the TP is a huge, elevated heat source to the middle troposphere, and that the sensible heat pump plays an important role in the regional climate, especially in the establishment, development, and variability of the South and East Asian monsoon (Ye 1981; Yanai et al. 1992; Wu et al. 2007; Wang et al. 2008; Lau et al. 2010; Liu et al. 2020b; Xu et al. 2022). Furthermore, recent studies have tackled the TP effect in upstream regions, such as North Africa (Lu et al. 2018; Nan et al. 2019; Chen et al. 2021). The TP LST/SUBT's role in global S2S precipitation prediction, however, has never been a subject in previous studies.

The LS4P-I experiment demonstrates that the spring TP LST/SUBT effects on June precipitation are not confined to the Yangtze River Basin that was found in a previous study (Xue et al. 2018), but it extends to many parts of the world. Figure 5 displays the difference between ensemble

means of 16 ESMs for the cold and warm cases. The figure shows that the imposed LST/SUBT initial condition over the TP that leads to cold May T2m has produced differences in June precipitation over many parts of the world. We define hotspots as the areas with a significant June precipitation impact in the model simulations due to the May TP cold temperature ($p < 0.10$ in t-test, dots in Fig. 5), which are also consistent with the observed anomaly (Fig. 1a). Based on this definition, eight hotspot regions are identified: (1) the SYRB, (2) northeast Asia, (3) northwest North America, (4) Southern Great Plains (SGP), (5) Central America, (6) northern South America, (7) western Sahel, and (8) East Africa (Fig. 5). For these hotspots, the observed lag relations as discussed in Xue et al. (2022) represent cause and effect.

To obtain a quantitative assessment of the TP LST/SUBT effect and its uncertainty among the ESMs, we select subregions defined by a latitude–longitude box covering each hotspot area based on the spatial distributions of maximum observed and simulated precipitation anomalies (see Fig. 5). The bar on each box represents the results in the sub-region of one selected ESM, the red bar is the observed anomaly, and the black bar corresponds to the ensemble mean difference. Among those hotspot regions, the ensemble members show the most consensus on drought in the SYRB. The cause of this drought has not been identified so far. As shown in the SYRB box, 12 models produced drought, while another 4 models produced values with the opposite sign but with very small magnitude, only 0.1–0.2 mm day^{-1}. The ensemble mean predicted about 42% of the drought anomaly (Fig. 5, Table 4). The results of the LS4P models for another hotspot, the SGP (Table 4), exhibit surprising consistency. Eleven models produced the observed pluvial wet anomaly, while five models produced negative anomalies, albeit with a very small magnitude. The ensemble mean captured 44% of the observed anomaly (Fig. 5, Table 4). It should be pointed out that the original objective of the LS4P-I was merely to check whether the ability of one ESM to produce drought in SYRB for a cold TP LST/SUBT (Xue et al. 2018) could be reproduced by other ESMs. The TP LST/SUBT effect on other parts of the world was not the initial focus of the LS4P-I modeling groups. As such, the consistency over the SGP is particularly impressive and reflects the current ability of state-of-the-art ESM to capture the most essential dynamic and physical processes.

A higher consensus was found in other hotspot regions, such as Northeast Asia, Northwest U.S./Southwest Canada, Central America, and northern South America. Similar to the SYRB and SGP, only 4 or 5 models produced an anomaly with a different sign than that in the observation, albeit with small magnitudes (Fig. 5, Table S1). Model uncertainties are relatively large only in two African hotspots: 7 models had opposite signs to that in the observations. Except for
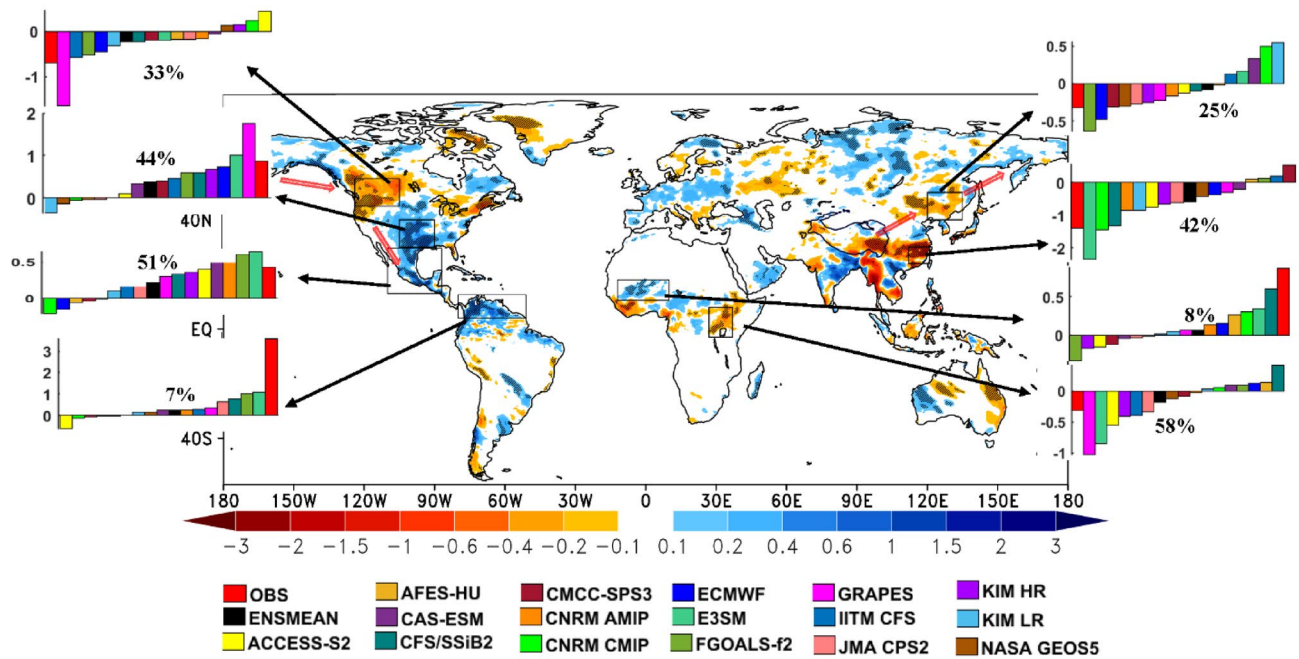
Fig. 5 LS4P-I ensemble mean June precipitation anomaly (mm day^{-1}) due to TP May LST/SUBT effects. Note: Each model is represented by a color bar. Red and black represent the observation anomaly and ensemble mean difference over the hotspot regions as defined in Table 5, respectively. The value in black shows the percentage of observed anomaly simulated by the ensemble mean

Table 5 Domain coordinates for statistics (LST/SUBT effects)

Sub-region	Coordinates for statistics
Southern Yangtze River Basin	112° E–121° E and 24° N–30° N
Northeast Asia	120° E–135° E and 40° N–52.8° N
East Africa	27° E–37° E and 3° S–8° N
Western Sahel	12° W–10° E and 10.5° N–18° N
Southern Great Plains	105° W–90° W and 30° N–40° N
Central America	110° W–87° W and 13° N–29.5° N
Northern South America	80° W–51° W and 4° N–12.5° N
Northwest North America	124° W–105° W and 45° N–55° N
North Hemisphere	180° W–180° E and 5° N–60° N
Global Land	180° W–180° E and 60° S–60° N

northern South America and western Sahel, ensemble means predict about a quarter to one half of the observed precipitation anomaly. In northern South America, the consensus among models is high. The magnitude of the observed anomaly in the region was quite large, however, and the TP effect seems to contribute little in the 2003 case. In the western Sahel, model uncertainty is relatively large, resulting in a weak anomaly in the ensemble mean (Table 5).

Five hotspot regions are located along the TRC wave train, and one is in its extension. Using reanalysis data of the May 200-hPa geopotential height (GHT) and observed T2m data from 1981 to 2015, a regression analysis

identified that the wave flux pattern progresses from the TP through northeast Asia and the Bering Strait to the western part of North America, which is referred to as the TRC wave train (Xue et al. 2022). The dashed arrows in Fig. 5 illustrate the TRC path. The heating change over the high mountain TP region modifies the phase, strength, and shape of this wave train, which may intrinsically exist in the midlatitude atmosphere along with the westerly jet probably due to the two high-elevation mountains, affecting the atmospheric circulation in its downstream region such as the west coast of North America. As a matter of fact, tropical–extratropical teleconnections that are caused by fluctuations large-scale heat sources and sinks in the Indo-Pacific region, such as El Niño in boreal summer, have been investigated in a number of studies (Lau and Weng 2002; Ding et al. 2011). Ding et al. (2011) identified two global teleconnection patterns: "the circumglobal teleconnection pattern, which is mainly a zonally oriented wave train along the westerly waveguide, and the western Pacific–North America pattern, which is a wave train emanating from the western Pacific monsoon trough", which is a wave train closely linked to the variations of Asian monsoon anticyclone. It is not clear how the unique features of TRC wave train interact/modify the aforementioned wave trains. In this content, the out-of-phase relation between TPI and RMI needs to be further investigated. It

Table 6 Domain coordinates for statistics (SST effects)

Sub-region	Coordinates for statistics
Horn of Africa	30° E–43° E and 6° N–13.5° N
North Europe	20° E–41° E and 57° N–68° N
Northern Yangtze River Basin	103° E–120° E and 29° N–37.5° N
US Midwest	103° W–86.5° W and 32.5° N–41.5° N
West Australia	114° E–130° E and 34° S–18° S
West Amazon Basin	76° W–69° W and 8° S–4° N

is interesting to notice that the consensus among ESMs is higher in the six identified hotspot regions along the TRC wave train path. The tropical northern South America is on the extension of the TRC path. The possible teleconnection between TP and northern South America has been detected in a paleo-climate study (Thompson et al. 2018), which identified two distinctive trans-Pacific events in the mid-fourteenth and late-eighteenth centuries in both locations from elevated aerosol concentrations in ice cores from the Peruvian Andes and the Tibetan Himalayas (Table 6).

In addition to the six hotspots already mentioned, another two are identified in the western Sahel and East Africa. The linkage between Northern African precipitation and TP topographic and thermal forcing have been investigated in a few recent studies (Lu et al. 2018; Nan

et al. 2019; Chen et al. 2021). By analyzing the summertime Tibetan tropospheric temperature (TTT) using reanalysis data, it was found that the TTT affects the zonal-vertical circulation between the western TP and Mediterranean Sea and meridional-vertical circulation over the Mediterranean Sea–Africa region, then precipitation in the central-eastern Sahel (Nan et al. 2019). Another study with various specified surface albedos over the TP found that various local anomalies in surface heating affected the South Asian high and generated a Rossby Wave response to impact upstream regions, such as North Africa (Lu et al. 2018). As mentioned earlier, due to limitations in the scope of this paper, mechanisms of TP effect on some of the global S2S precipitation will be discussed in a separate paper. In the next section of this paper, we focus on how the LST/SUBT affects the East Asian monsoon precipitation.

5 Mechanisms of the LST/SUBT effects on East Asian monsoon

The LST/SUBT impact as shown in Fig. 5 is the result of the cold TP May temperatures. Figure 6 displays the relationship between differences in May TP T2m and those in several other variables between the ensemble means of the cold and warm cases. The correlation coefficients of the linear regression and statistical significance between these
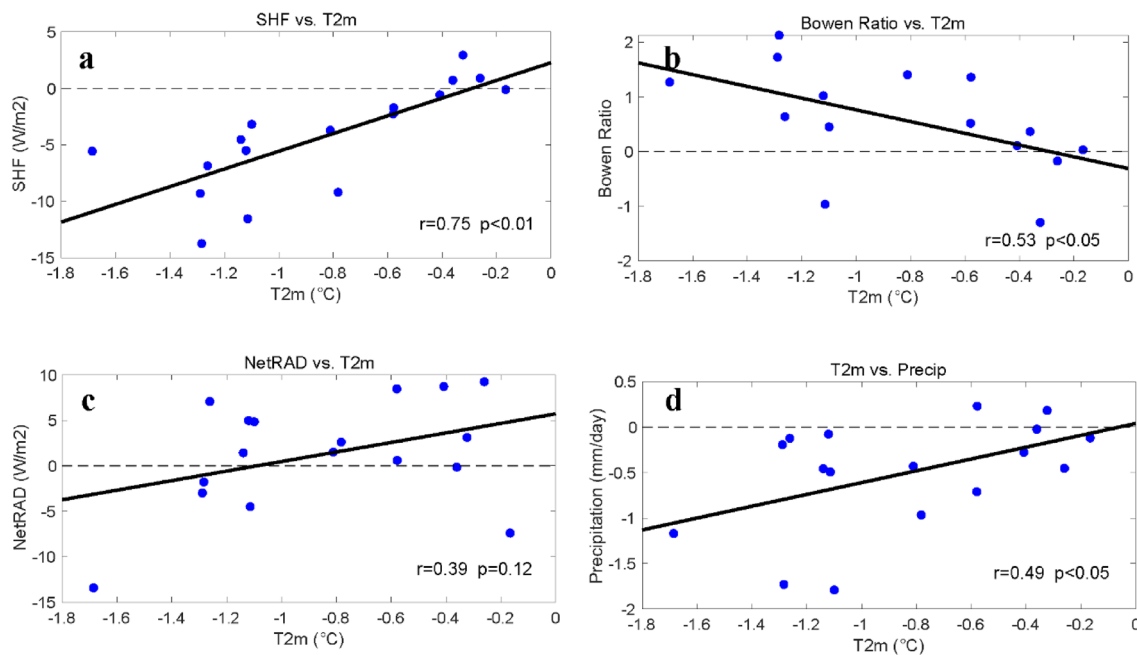
Fig. 6 Scatter plots T2m difference for May 2003 over the TP versus other variable differences due to LST/SUBT effects. **a** Sensible heat flux (W m^{-2}). **b** TP May Bowen ratio over the TP for May, **c** Net radiation (W m^{-2}) over the TP for May, and **d** Precipitation (mm day^{-1}) over the southern Yangtze River Basin (103° E–119.5° E and 26.5° N–32° N) for June. Each dot represents an individual model
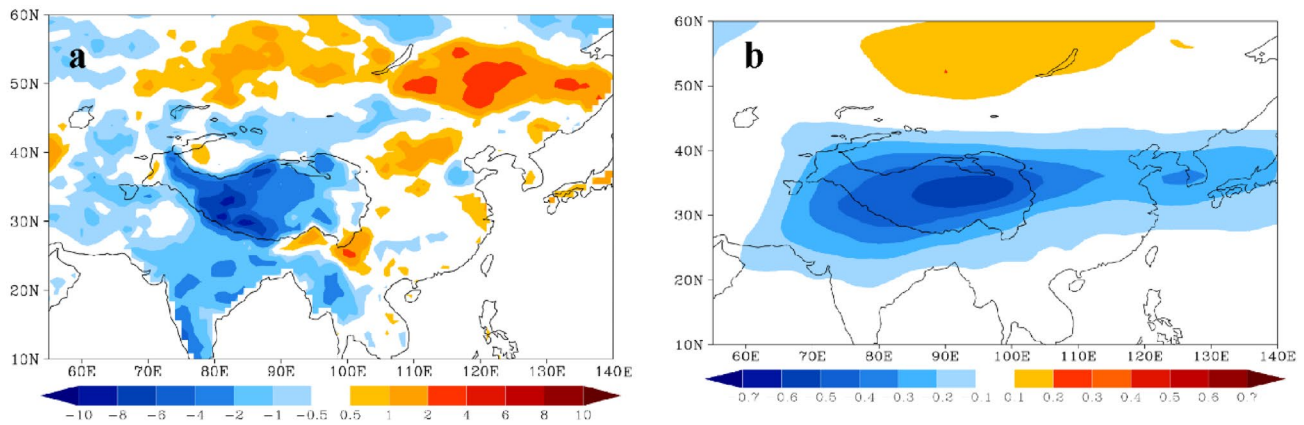
Fig. 7 May 2003 ensemble mean difference due to LST/SUBT effects. **a** Surface sensible heat flux (W m^{-2}); **b** air temperature (°C) at 300 hPa

two differences are also listed in each panel of the figure. Figure 6d demonstrates that there is a significant linear correlation between simulated May T2m differences over the TP and June precipitation differences over the SYRB, suggesting the model's TP T2m simulation impacts the model's performance in predicting precipitation anomalies over that region. We have not found such a simple linear relationship for the other hotspot regions. Apparently, more factors contribute to the remote effect discussed here.

In reference to the relationships among TP T2m with other variables over the TP, the differences of the sensible heat flux and T2m have the highest correlation with highest significance compared with other variables (Fig. 6a). This is because the T2m influences the temperature gradient between land surface and atmosphere as well as the stability conditions in the surface layer, which directly influence the sensible heat flux. The T2m and the Bowen Ratio (i.e., the ratio of sensible to latent heat fluxes at the surface) also have significant but weaker correlation coefficient (Fig. 6b). In addition, T2m influences the long wave radiation exchange between surface and atmosphere. The influence is not that significant for the total net radiation (i.e., the sum of net shortwave and net longwave radiation) (Fig. 6c).

Cold May T2m and lower sensible heat from the surface over the TP (Figs. 3b and 7a) generates cold temperatures in the atmospheric column over the region, as displayed in Fig. 7b for 300 hPa. The cold May T2m persisted until June, although it weakened in time (Fig. 3b). The lowest values in the cold temperature band in May are located along about 32° N (Fig. 7a), which generated a negative meridional temperature gradient to the south of and a positive gradient to the north of that latitude. On the basis of the thermodynamics of atmospheric circulation, a negative meridional temperature gradient will generate westerly thermal wind. As such, the westerly zonal wind at 200 hPa becomes stronger/weaker to the south/north of

around 32° N, respectively, indicating a shift of westerly jet to the south in May and June (Fig. 8a, b). Following the zonal wind change as shown in Fig. 8a, b, a strong positive vorticity band was created between ~ 30–40° N in Fig. 8c, d, which is consistent with the relation in the relative vorticity equation. Meanwhile, a negative vorticity band was induced to the north of that band. Furthermore, the geopotential height difference at 200 hPa also made corresponding change as shown in Fig. 8e, f, due to the quasi-geostrophic relationship between wind and geopotential height in midlatitudes. An eastward shift of a strong positive vorticity and negative geopotential height center from the TP to the east during May and June is apparent in Fig. 8c–f.

To examine the effect of imposed LST/SUBT anomaly over the TP on the characteristics of eastward propagating wave energy, which can further affect the downstream East Asian Summer Monsoon (Lee et al. 2013; Ren et al. 2021), we look at the eddy kinetic energy (EKE) of transient eddies. Transient eddy activities play a principal role in transporting heat, momentum, and moisture in midlatitudes (Hoskins and Hodges 2002; Ren et al. 2010; Diallo et al. 2022).

The EKE is defined as follows (Wallace et al. 1988; Hoskins and Valdes 1990):

$$EKE = \frac{\overline{u'^2} + \overline{v'^2}}{2}$$

where u' and v' represent the transient disturbance of the zonal and meridional wind, respectively, and over-bar denotes monthly means. Disturbances are calculated from the daily u (v) by subtracting their monthly mean values. Figure 9a, b display temporal-zonal cross-section of EKE and vorticity at 200 hPa averaged over the latitude band from 27° N to 40° N which covers the TP. After producing the
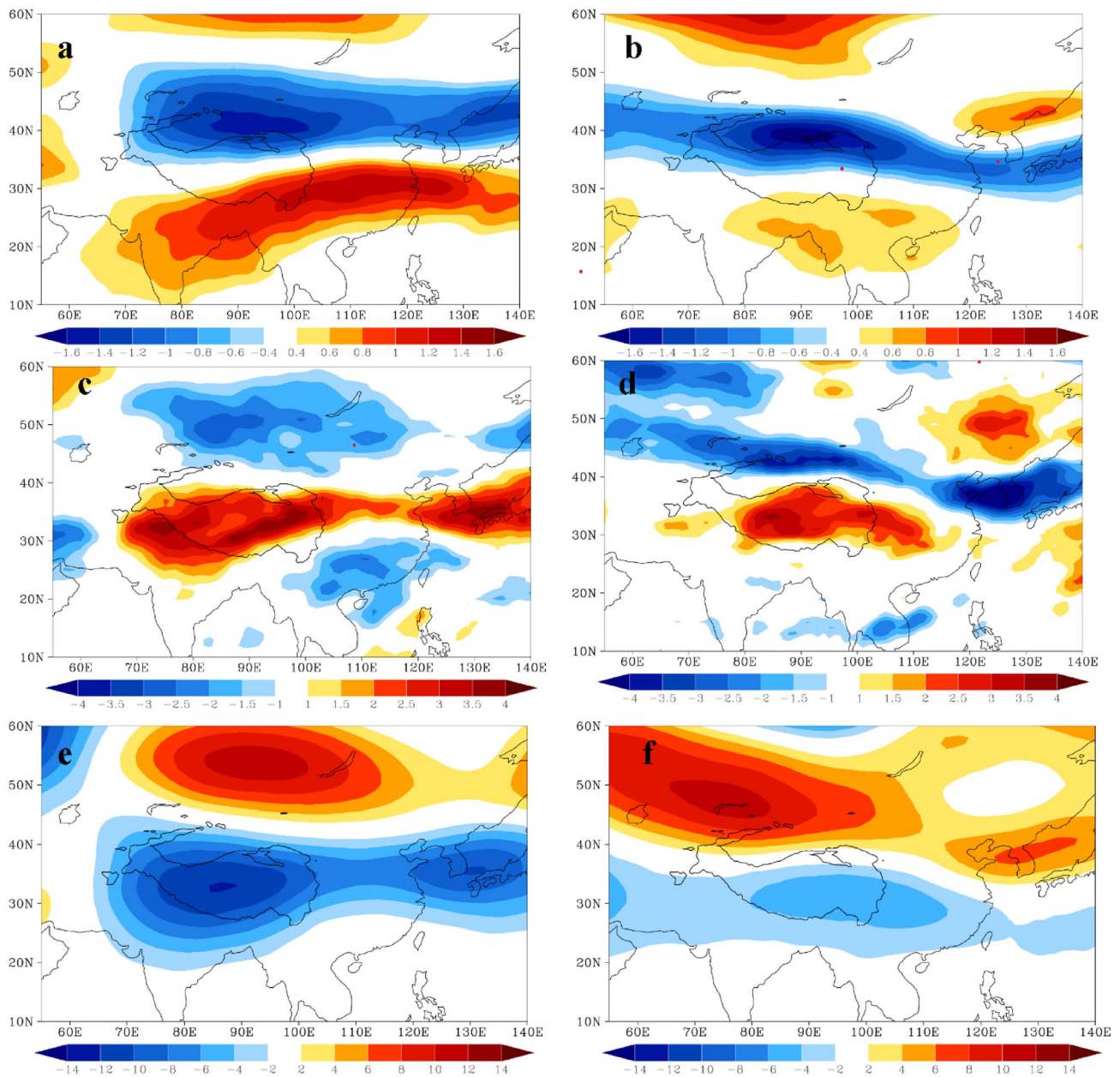
Fig. 8 a Ensemble mean differences at 200 hPa of zonal wind speed (m s^{-1}) for May 2003 due to the LST/SUBT effects. **b** Same as **a**, except for June 2003. **c, d** Same as **a** and **b**, except for the vorticity difference ($\times 10^{-6}$ s^{-1}), respectively. **e, f** Same as **a** and **b**, except for the geopotential height difference (gpm), respectively

LST/SUBT anomaly over the TP, the positive (i.e., stronger than average) transient eddy anomalies on a synoptic time-scale and bi-weekly time scale from TP move eastward. In particular, wave energy propagates eastward during the late part of May (Fig. 9a), which can cause the circulation anomalies over the downward east Asian region by atmospheric internal dynamic processes (Ren et al 2015; Wang et al 2019; Zhu et al 2022; Zhao et al 2022). Our simulation demonstrated that the LST/SUBT can lead to the adjustment of waves in the westerlies and provide energy for the

upper-level vorticity (Fig. 9b) and geopotential height anomalies to move eastward during that period.

As a result of such circulation changes, the divergence and convergence also change. In view of the baroclinicity vertical structure, the horizontal wind divergence and convergence in the lower and upper troposphere have opposite signs over the eastern Asian lowland plains (Li et al. 2014; Ren et al. 2015; Lee et al. 2021; Diallo et al. 2022). The positive vorticity and lower geopotential height shown in Fig. 8c–f are associated with convergence in the upper
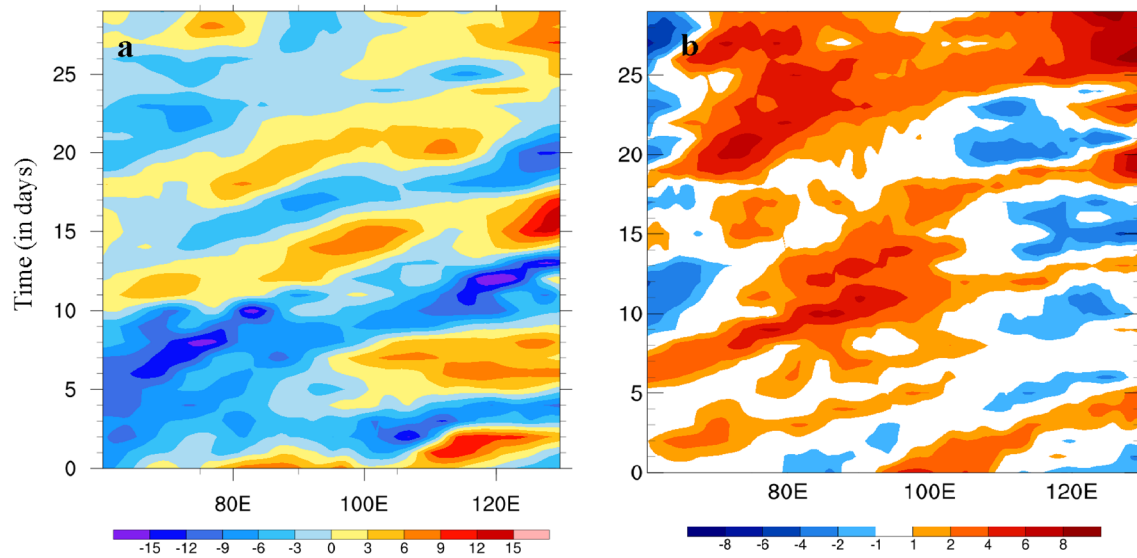
Fig. 9 Time-longitude cross-section of differences of **a** Eddy kinetic energy (m^2 s^{-2}) and **b** vorticity ($\times 10^{-6}$ s^{-1}) due to LST/SUBT effects at 200 hPa during May 2003 averaged over latitude 27° N–40° N
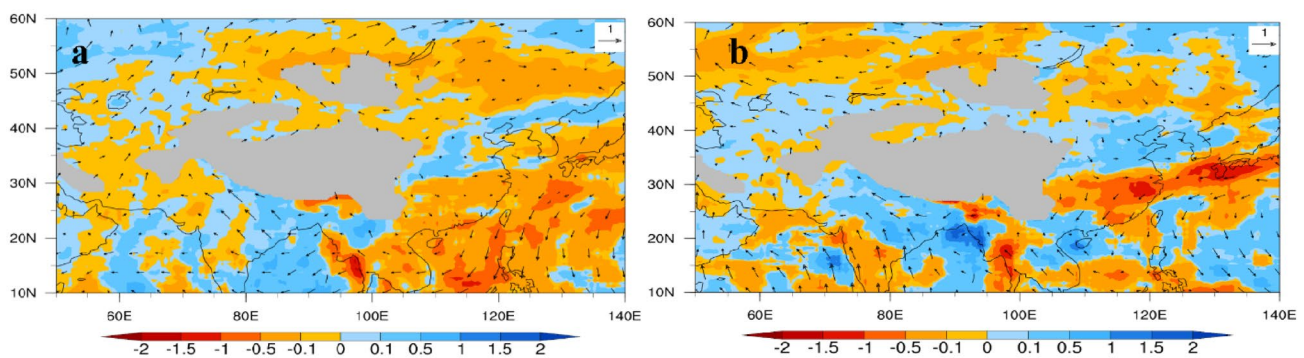
Fig. 10 Vertical integrated moisture flux convergence (mm day^{-1}) difference due to LST/SUBT effects superimposed with 850 hPa wind vector. **a** May; **b** June

troposphere (not shown). In the lower troposphere, there would be a divergence, which is clearly demonstrated in Fig. 10. The southwestward wind vectors at 850 hPa in June in the SYRB exhibit an anticyclonic structure that weakens the summer monsoon flow from the Bay of Bengal and South China Sea (Fig. 10b). The reduced vertically integrated moisture flux convergence, to which the lower troposphere moisture makes the major contribution, over the SYRB is consistent with drought in that area.

6 SST effect of precipitation

The SST's role in climate and weather prediction has been investigated in numerous studies. The purpose of presenting the results of the SST's effect on the May and June precipitation herein is to compare its effect with the TP LST/

SUBT effect using the same state-of-the-art ESMs. The year 2003 was a moderate El Niño year. By May and June 2003, although the southern oceans were still very warm, the SST in the eastern and northern Pacific was relatively cold (Fig. S3). In Exp-SST, the daily May and June 2003 SST was replaced by the daily climatological SST. Thirteen LS4P-I ESMs submitted Exp-SST results. Only one ESM (CNRM CMIP) among these 13 models predicts the ocean temperature. Nevertheless, the SST differences of the 13-ESM ensemble mean between Exp-CTRL and Exp-SST have very similar SST anomaly patterns as observed (Fig. 11).

The differences between Exp-CTRL and Exp-SST illustrate the SST effect (Figs. 4c and 12). There is speculation that the T2m anomaly in the TP is merely a product of the SST effect. The differences between T2m in Exp. CTRL and Exp. SST are shown in Fig. 4c. The SST anomalies in
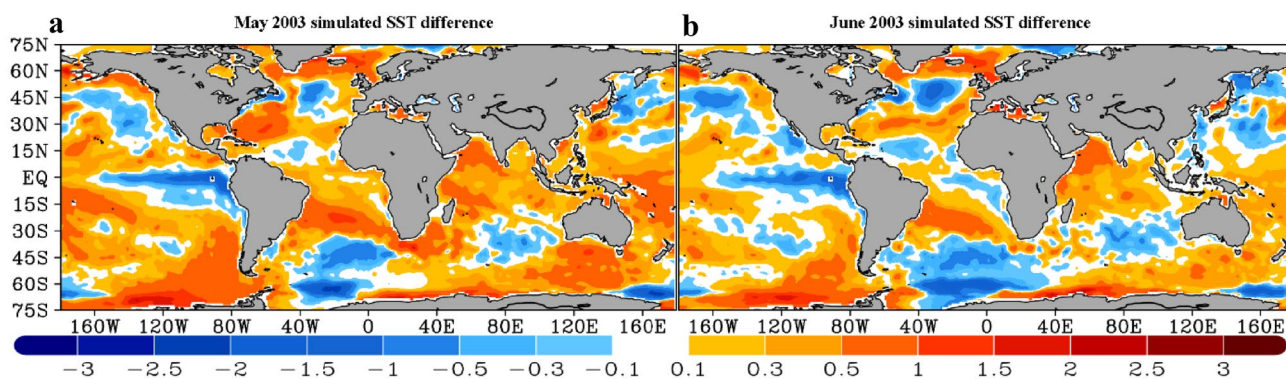
Fig. 11 LS4P-I model ensemble mean SST difference (°C) between Exp-CTRL and Exp-SST for **a** May and **b** June 2003. Note: Over polar regions, the SST represents the sea ice temperature
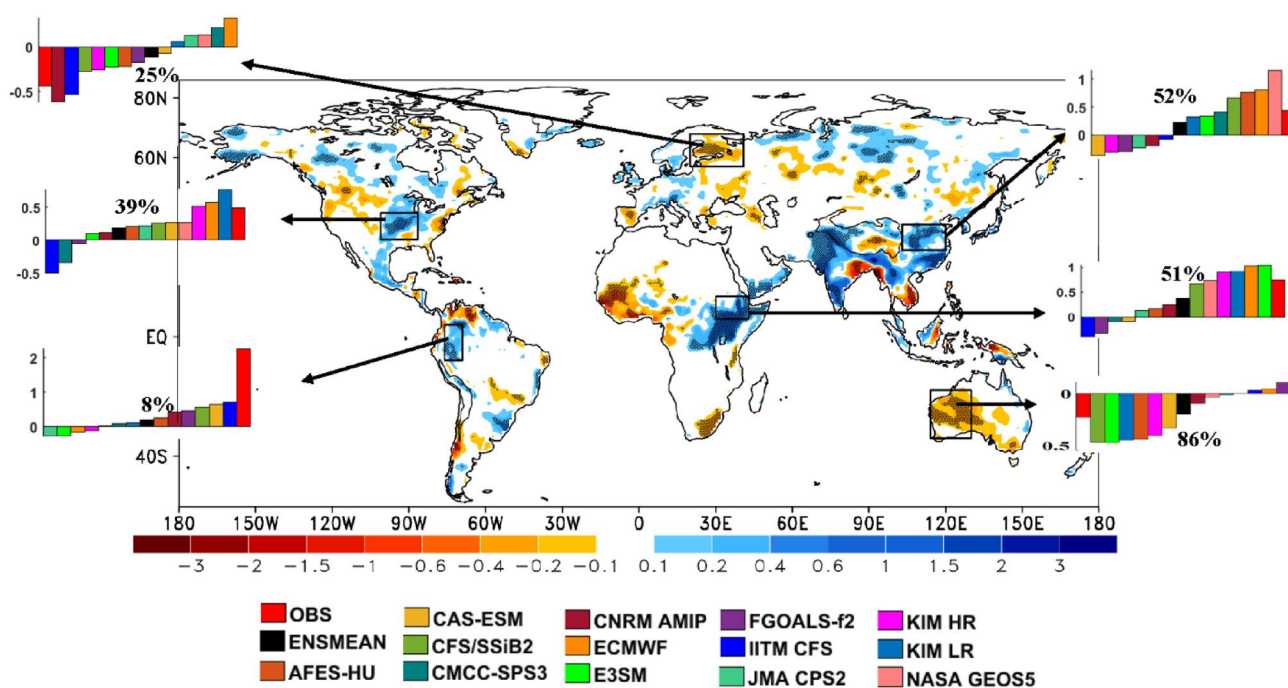

Fig. 12 Ensemble mean of June precipitation anomaly (mm day^{-1}) due to SST effects. Note: each model is represented by a color bar. Red and black represent the observation anomaly and ensemble mean difference over the regions defined by Table 6, respectively. The value in black shows the percentage of observed anomaly simulated by the ensemble mean

2003 are associated with a warm TP, which is opposite in sign to the observed TP T2m anomaly. As expected, the SST has significant impacts on the S2S precipitation prediction. Similar to the definition of LST/SUBT hotspots, six regions are identified where the SST anomalies produce significant precipitation differences which are also consistent with the observed June 2003 precipitation anomalies. These six regions are (1) the U.S. Midwest, (2) west Amazon Basin, (3) Horn of Africa, (4) Western Australia, (5) Northern Yangtze River Basin, and (6) Northern Europe (Fig. 12). The former three of these regions partially overlap with the

TP LST/SUBT hotspots, indicating that both LST/SUBT and SST play roles in precipitation anomalies with the same sign in these areas, i.e., the forcings work in the same direction. In the Northern Yangtze River Basin, Central America, northwestern North America, and northeastern Asia, both forcings produce the same sign of anomalies, but only one of them produces statistically significant results. At this stage, it is unclear whether these non-significant results from one forcing are due to model deficiencies or whether the second forcing really plays a secondary role. For the regions mentioned above, the two effects may be hard to distinguish. In

Fig. 13 **a** Ensemble mean of June 2003 Vertical Integrated Moisture Flux Convergence difference (mm day^{-1}) due to TP LST/SUBT effects and **b** same as **a** but due to SST effects
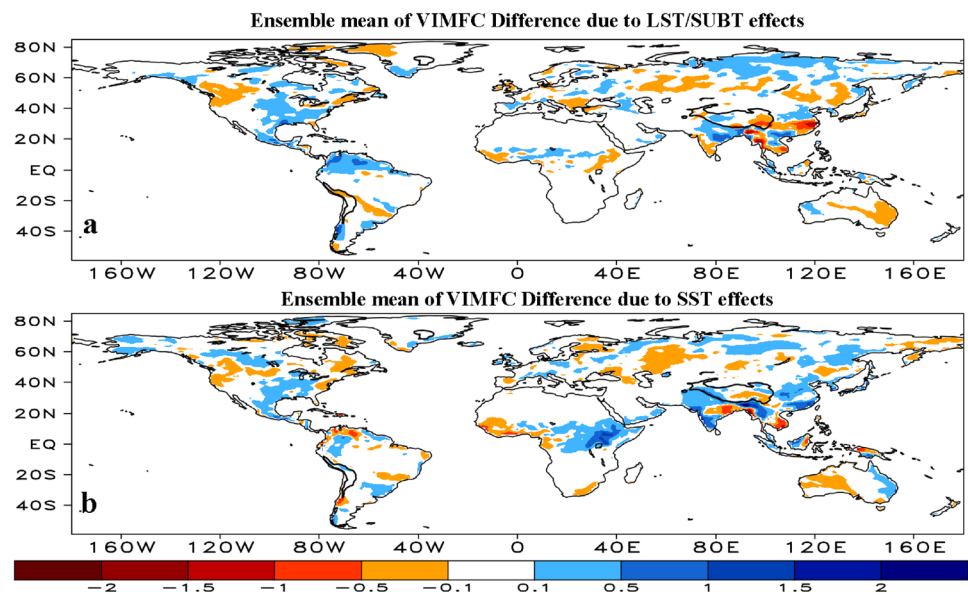
Western Australia, Northern Europe, and the western Sahel, the SST and LST/SUBT produce anomalies with opposite signs, indicating that their effects interfere destructively. Again, we are unable to confirm if such an interference is due to model deficiencies or if it reflects the real nature of these forcings' effect.

Except for the north Yangtze River Basin, only four or five ESMs among 13 have opposite signs compared with the ensemble mean. However, the magnitudes of these ESMs' results with opposite anomalies are generally larger than the Exp-LST/SUBT. It seems the Exp-LST/SUBT exhibits less uncertainty compared with Exp-SST in the 2003 case. The SST also produced about 25–50% of the observed precipitation anomaly in the northern Yangtze River Basin, Horn of Africa, North Europe and the U.S. Midwest. In the western Amazon and Western Australia, the observed anomaly is very large/small, and the ensemble mean produces relatively small/large anomalies, respectively. Exp-SST only involved 13 ESMs (Table 2). We use the same 13 ESMs to draw a figure (Fig. S4) to show the TP LST/SUBT effect. Figure S4 and Fig. 5 show generally consistent results. Overall, the 13 ESMs selected produce better precipitation anomalies over the LST/SUBT hotspot regions. In particular, the northern Yangtze River Basin's pluvial flood condition is well simulated. In Sect. 4.2, based on 16 ESMs results, the Northern Yangtze River Basin had not been selected as a hotspot for the LST/SUBT effect.

In Sect. 5, we have shown the TP LST/SUBT influence on East Asian summer precipitation through its influence on atmospheric circulation and moisture flux convergence. Both TP LST/SUBT and SST produce remote impacts through their influence on the large-scale atmospheric circulation. Figure 13 shows the vertical integrated moisture flux

convergence (MFC) for both the LST/SUBT and SST effects. The differential equation used to calculate the moisture flux convergence is sensitive to temporal resolution, sample size, etc., and required high horizontal resolutions (Berbery and Rasmusson 1999). The global models' horizontal and vertical resolutions would cause large computational errors. We used the difference between monthly precipitation and evaporation to quantitatively represent vertically integrated Moisture flux convergence [as done in other studies (Xue et al. 2010)] Furthermore, Oshima et al. (2015) shows that this representation is quite accurate. The patterns of the differences in integrated moisture flux convergence/divergence in Fig. 13 are very consistent with those in precipitation differences shown in Figs. 5 and 12, respectively. The changes in moisture convergence/divergence by the atmospheric circulation change modulated by the surface heating change in the TP or SST play a dominant role in this study.

7 Discussion and summary

Due to the importance of S2S precipitation prediction in weather/climate research and applications—as well as to the well-known fact that S2S prediction skill has remained stubbornly low for years—the WCRP/WRRP has listed S2S prediction as a "weather–climate prediction desert" with a high priority (Robertson et al. 2018; Merryfield et al. 2020). The GEWEX/LS4P community effort aims to explore an innovative approach to tackle this issue using high mountain temperature as a new source for S2S predictability. The observational data, especially from the TP, have provided useful information to support this approach, especially the discovery of an out-of-phase relationship between the TPI

and RMI and a TRC wave train from the TP to the western part of North America. The global teleconnection patterns in Northern summer through barotropic instability and a wave train associated with the westerly jet stream have been extensively investigated (Simmons et al. 1983; Lau and Peng 1991; Ding and Wang 2005), including the linking of summertime precipitation variability over East Asia and North America (Lau and Weng 2002; Lau et al. 2004). In these studies, the teleconnection signals stemmed from Rossby wave dispersion associated with fluctuations of large-scale heat sources and sinks in the oceans, such as El Nino. In this study, the TRC wave train identifies specific "mountain sources" as key in enhancing the S2S prediction around the globe. The high mountain heating sources over the Tibetan Plateau and the Rocky Mountain in early summer are key drivers of S2S predictability around the globe, through barotropic instability and excitation of Rossby wave dispersion phase-locked to the seasonal variation of the East Asian jet. A TRC wave train identified in this study is likely to play a fundamental role. In addition to forcing by SST anomalies, the surface heating over high mountains also plays an important role in generating circum-global teleconnections. The special mechanisms at work for the teleconnections need to be further investigated in LS4P Phase II (LS4P-II).

The LS4P-I designed several experiments to test whether the high mountain LST/SUBT provides an additional source for the S2S prediction. The present paper reports some key discoveries resulting from more than 3 years of community effort. With the LS4P-I initialization method (Xue et al. 2021), the observed TP surface temperature anomaly has been partially produced and 8 hotspot regions in the world have been identified where June precipitation is related in a statistically significant manner to anomalies of TP May T2m. The TP LST/SUBT effect has produced about 25–50% of the observed precipitation anomaly in most of the hotspot regions. Also, the ESMs have shown more consistency in the hotspot regions along the TRC wave train path. The modification/shift in the westerly jet and other circulation characteristics in the upper troposphere over the TP induced by the TP surface heating generate eastward propagating wave energy. Due to the baroclinicity vertical structure in the troposphere above the East Asian lowland plains, the anticyclone and moisture divergence at low levels created the conditions for the 2003 drought in the SYRB. For comparison, the global SST effect in the 2003 case had significant impacts in 6 regions, explaining about 25–50% of observed precipitation anomalies over most of these regions. These findings suggest that the TP LST/SUBT is a first order source of the S2S predictability, which is comparable to the ocean conditions.

Many issues must be further addressed in order to realize the full potential of the novel developments presented in this paper. In the following we list a few major ones.

(1) The land parameterization and reanalysis data that is used for the ESM's initial and boundary conditions have been considered as the main causes for the LS4P-I models' inability to produce the observed anomalies (Xue et al. 2021). This study shows that even with improved initialization, the LS4P-I ensemble mean is still unable to fully produce the observed TP T2m anomaly. The initialization is based on the observed May T2m anomaly (− 1.4 °C) and model bias. Since most models have positive biases, the absolute value of imposed mask (ΔT) on average will be larger than 1.4 °C. However, Fig. 3b shows that by May 1, which is only a few days after initialization, the ensemble mean difference is only − 1 °C. With such quick loss of initial soil temperature anomaly, the inconsistency in reanalysis data probably plays a dominant role. Our analysis (Xue et al. 2021) has revealed the weakness of reanalysis data over the TP, where very little station data are available for reanalysis. The nudging approach (Tang et al. 2019) has shown promise in improving atmosphere initial conditions over high mountain areas and is worth further investigations to improve both atmosphere and land initial conditions.

(2) In some regions, such as in the Eurasian continent and India, the statistical analysis revealed significant lag correlations between precipitation and TP T2m (Xue et al. 2022). The LS4P-I ensemble mean, however, fails to produce such relationships. This issue deserves further investigation, such as that done by Saha et al. (2023). Furthermore, the simulated TP LST/SUBT difference of the LS4P-I ensemble mean produces significant June precipitation anomalies in some regions, such as coastal West Africa, southeast TP, and Western Europe, but with an opposite sign compared to the observations. These regions are not defined as hotspots in this study. It is unclear whether the issues raised above are due to model deficiencies, including a failure in producing the full TP May T2m anomaly, or if some other processes involved which are more important than the TP LST/SUBT effect. It would be interesting to perform sensitivity simulations (e.g., with initial perturbations in the atmospheric and/or land states) with large ensemble members using individual models and assess how robust the multi-model ensemble mean results are in the hotspot regions versus in the above regions.

(3) The land–atmosphere interaction studies performed so far have been focused on the local land surface/atmosphere feedbacks with a substantial number of publications and large amount of experience. In the LS4P research, we explore the remote effect of land surface conditions. There is a need to further study the com-

bined remote and local effect due to snow, soil moisture, vegetation, etc.

With the completion of the LS4P-I, the LS4P-II has been launched in 2023 to further explore outstanding S2S prediction issues associated with the high mountain LST/SUBT effect. The LS4P-II will focus on the Western U.S. (mainly the Rocky Mountains region), and the effects of its land temperature on precipitation over North and Central America and elsewhere, particularly the atmospheric teleconnections between North America and East Asia. For the LS4P Phase II, the year 1998 has been selected because it features a very cold spring in the Western U.S., severe summer drought in Texas and Oklahoma (Hong and Kalnay 2002), very warm spring over the TP, and severe summer flooding in the Yangtze River Basin (Diallo et al. 2022). More information on the Phase II experiments, including its protocol, can be found on the LS4P website (http://ls4p.geog.ucla.edu).

Up until now, land–atmosphere interaction studies have largely focused on the local feedbacks between land and atmosphere. A lack of observational data has presented a crucial limitation. In the LS4P experiment, the T2m, which has the highest quality among measured land variables and the longest meteorological observational record with global coverage and dense measurements, has been applied as a reference to explore the possible remote effects of large-scale spring LST/SUBT anomaly over high mountains on summer precipitation anomalies. Our preliminary studies have stimulated research on the remote effect of land processes in other regions and seasons (Shukla et al. 2019; Yang et al. 2021, 2022; Qiu et al. 2022; Xu et al. 2022; Saha et al. 2023). The LS4P approach proposes a new front in S2S prediction to complement other existing approaches to substantially improve S2S prediction. We hope LS4P-I activities can raise further scientific questions and open a new gateway for more research with various approaches for a better understanding of the roles and mechanisms of land surface processes in weather/climate prediction, S2S predictability in particular.

Declarations

References

Bao Q, Wu X, Li J, He B, Wang X, Liu Y, Wu G (2019) Outlook for El Niño and the Indian Ocean Dipole in autumn-winter 2018–2019. Chinese Sci Bull 64:73–78. https://doi.org/10.1360/N972018-00913

Bauer P, Thorpe A, Brunet G (2015) The quiet revolution of numerical weather prediction. Nature 525:47–55. https://doi.org/10.1038/nature14956

Berbery EH, Rasmusson EM (1999) Mississippi moisture budgets on regional scale. Mon Weather Rev 127:2654–2673

Branstator G (2014) Long-lived response of the midlatitude circulation and storm tracks to pulses of tropical heating. J Clim 27:8809–8825

Charney J, Quirk WJ, Chow S-H, Kornfield J (1977) A comparative study of the effects of albedo change on drought in semi-arid regions. J Atmos Sci 34:1366–1385

Chen J, Ma Z, Li Z, Shen X, Su Y, Chen Q, Liu Y (2020) Vertical diffusion and cloud scheme coupling to the Charney-Phillips vertical grid in GRAPES global forecast system. Q J Roy Meteor Soc 146:2191–2204. https://doi.org/10.1002/qj.3787

Chen Z, Wen Q, Yang H (2021) Impact of Tibetan Plateau on North African precipitation. Clim Dyn 57:2767–2777. https://doi.org/10.1007/s00382-021-05837-2

DelSole T, Trenary L, Tippett MK, Pegion K (2017) Predictability of week-3–4 average temperature and precipitation over the contiguous United States. J Clim 30:3499–3512. https://doi.org/10.1175/JCLI-D-16-0567.1

Diallo I, Xue Y, Li Q, De Sales F, Li W (2019) Dynamical downscaling the impact of spring Western US land surface temperature on the 2015 flood extremes at the Southern Great Plains: effect of domain choice, dynamic cores and land surface parameterization. Clim Dyn 53:1039–1061. https://doi.org/10.1007/s00382-019-04630-6

Diallo I, Xue Y, Chen Q, Ren X, Guo W (2022) Effects of spring Tibetan plateau land temperature anomalies on early summer floods/droughts over the monsoon regions of South East Asia. Clim Dyn. https://doi.org/10.1007/s00382-021-06053-8

Ding Q, Wang B (2005) Circumglobal teleconnection in the Northern Hemisphere summer. J Clim 18:3483–3505

Ding Q, Wang B, Wallace JM, Branstator G (2011) Tropical-extratropical teleconnections in boreal summer: observed interannual variability. J Clim 24:1878–1896

Fan Y, Van den Dool H (2008) A global monthly land surface air temperature analysis for 1948–present. J Geophys Res Atmos 113:D01103. https://doi.org/10.1029/2007JD008470

Golaz J-C, Caldwell PM, Van Roekel LP et al (2019) The DOE E3SM coupled model version 1: overview and evaluation at standard resolution. J Adv Model Earth Syst 113:D01103. https://doi.org/10.1029/2018MS001603

Han S, Shi CX, Xu B, Sun S, Zhang T, Jiang L, Liang X (2019) Development and evaluation of hourly and kilometer resolution retrospective and real-time surface meteorological blended forcing dataset (SMBFD) in China. J Meteorol Res 33:1168–1181. https://doi.org/10.1007/s13351-019-9042-9

Harris I, Jones PD, Osborn TJ, Lister DH (2014) Updated high-resolution grids of monthly climatic observations—the CRU TS3.10 Dataset. Int J Climatol 34:623–642. https://doi.org/10.1002/joc.3711

Hong S-Y, Koo M, Jang J, Esther Kim J, Park H, Joh M, Kang J, Oh T (2013) An evaluation of the system software dependency of a global spectral model. Mon Wea Rev 141:4165–4172. https://doi.org/10.1175/MWR-D-12-00352.1

Hong S-Y, Kwon YC, Kim T-H, Kim J-EE, Choi S-J, Kwon I-H, Kim J, Lee E-H, Park R-S, Kim D-II (2018) The Korean Integrated Model (KIM) system for global weather forecasting, Asia-Pac. J Atmos Sci 54:267–292. https://doi.org/10.1007/s13143-018-0028-9

Hong S-Y, Kalnay E (2002) The 1998 Oklahoma-Texas drought: mechanistic experiments with NCEP global and regional models. J Clim 15:945–963

Hoskins BJ, Hodges KI (2002) New perspectives on the Northern Hemisphere winter storm tracks. J Atmos Sci 59:1041–1061

Hoskins BJ, Valdes PJ (1990) On the existence of storm-tracks. J Atmos Sci 47:1854–1864

Hudson D, Alves O, Hendon HH, Marshall AG (2011) Bridging the gap between weather and seasonal forecasting: intraseasonal forecasting for Australia. Q J R Meteorol Soc 137:673–689. https://doi.org/10.1175/MWR-D-13-00059.1

Johnson SJ, Stockdale TN, Ferranti L, Balmaseda MA, Molteni F, Magnusson L, Tietsche S, Decremer D, Weisheimer A, Balsamo G, Keeley SPE, Mogensen K, Zuo H, Monge-Sanz BM (2019) SEAS5: the new ECMWF seasonal forecast system. Geosci Model Dev 12:1087–1117. https://doi.org/10.5194/gmd-12-1087-2019

Kirtman B, Min D, Infanti JM et al (2014) The North American Multimodel Ensemble: phase-1 seasonal-to-interannual prediction; phase-2 toward developing intraseasonal prediction. Bull Am Meteorol Soc 95:585–601. https://doi.org/10.1175/BAMS-D-12-00050.1

Koster RD, Dirmeyer PA, Guo Z et al (2004) Regions of strong coupling between soil moisture and precipitation. Science 305:1138–1140

Lau WKM, Peng L (1991) Dynamics of atmospheric teleconnections during the Northern summer. J Clim 2:140–158

Lau WKM, Weng H (2002) Recurrent teleconnection patterns linking summertime precipitation variability over East Asia and North America. J Meteorol Soc Jpn 80:1309–1324

Lau WKM, Lee JY, Kim KM, Kang IS (2004) The North Pacific as a regulator of summertime climate over Eurasian and North America. J Clim 17:819–833

Lau WKM, Kim M-K, Kim K-M, Lee W-S (2010) Enhanced surface warming and accelerated snow melt in the Himalayas and Tibetan Plateau induced by absorbing aerosols. Environ Res Lett 5:025204. https://doi.org/10.1088/1748-9326/5/2/025204

Lee S-S, Lee J-Y, Ha K-J, Wang B, Kitoh A, Kajikawa Y, Abe M (2013) Role of the Tibetan Plateau on the annual variation of mean atmospheric circulation and storm-track activity. J Clim 26:5270–5286. https://doi.org/10.1175/JCLI-D-12-00213.1

Lee J, Xue Y, De Sales F, Diallo I, Marx L, Ek M, Sperber KR, Gleckler PJ (2019) Evaluation of multi-decadal UCLACFSv2 simulation and impact of interactive atmospheric-ocean feedback on global and regional variability. Clim Dynam 52:3683–3707. https://doi.org/10.1007/s00382-018-4351-8

Li S, Robertson AW (2015) Evaluation of submonthly precipitation forecast skill from global ensemble prediction systems. Mon Weather Rev 143:2871–2889. https://doi.org/10.1175/MWR-D-14-00277.1

Li L, Zhang R, Wen M, Liu L (2014) Effect of the atmospheric heat source on the development and eastward movement of the Tibetan Plateau vortices. Tellus A 66:24451. https://doi.org/10.3402/tellusa.v66.24451

Li X, Che T, Li X, Wang L, Duan A, Shangguan D, Pan X, Fang M, Bao Q (2020) CAS earth poles: big data for the three poles. Bull Am Meteorol Soc 101:E1475–E1491. https://doi.org/10.1175/BAMS-D-19-0280.1

Lin Z-H, Yu Z, Zang H, Wu C-L (2016) Quantifying the attribution of model bias in simulating summer hot days in China with IAP AGCM 4.1. Atmos Ocean Sci Lett 9:436–442

Lin YL, Huang XM, Liang YS, Qin Y, Xu SM, Huang WY, Xu FH, Liu L, Wang Y, Peng Y R, Wang L, Xue W, Fu HH, Zhang GJ, Wang B, Li RZ, Zhang C, Lu H, Yang K, Luo Y, Bai YQ, Song Z, Wang M, Zhao W, Zhang F, Xu JH, Zhao X, Lu C, Luo Y, Hu Y, Tang Q, Chen D, Yang GW, Gong P (2019) The Community Integrated Earth System Model (CIESM) from Tsinghua University and its plan for CMIP6 experiments. Clim Change Res 15:545–550. https://doi.org/10.12006/j.issn.1673-1719.2019.166

Lin Y, Huang X, Liang Y, Qin Y, Xu S, Huang W, Xu F, Liu L, Wang Y, Peng Y, Wang L, Xue W, Fu H, Zhang GJ,Wang B, Li R, Zhang C, Lu H, Yang L, Luo Y, Bai Y, Song Z, Wang M, Zhao W, Zhang F, Xu J, Zhao X, Lu C,Chen Y, Luo Y, Hu Y, Tang Q, Chen D, Yang G, Gong P (2020) Community integrated earth system model (CIESM): description and evaluation. J Adv Model Earth Sys 12:e2019MS002036.https://doi.org/10.1029/2019MS002036

Liu Y, Xue Y, Li Q, Lettenmaier D, Zhao P (2020a) Investigation of the Variability of near-surface temperature anomaly and its causes over the Tibetan Plateau. J Geophys Res 125:e2020JD032800. https://doi.org/10.1029/2020jd032800

Liu YM, Lu M, Yang H, Duan A, He B, Yang S, Wu G (2020b) Land–atmosphere–ocean coupling associated with the Tibetan Plateau and its climate impacts. Natl Sci Rev 7:534–552. https://doi.org/10.1093/nsr/nwaa011

Lu MM, Yang S, Li ZN, He B, He S, Wang Z (2018) Possible effect of the Tibetan Plateau on the 'upstream' climate over West Asia, North Africa, South Europe and the North Atlantic. Clim Dyn 51:1485–1498

Ma YM, Kang SC, Zhu LP, Xu BQ, Tian LD, Yao TD (2008) Tibetan observation and research platform atmosphere-land interaction over a heterogeneous landscape. Bull Am Meteorol Soc 89:1487–1492

MacLachlan C, Arribas A, Peterson D, Maidens A, Fereday D, Scaife AA, Gordon M, Vellinga M, Williams A, Comer RE, Camp J, Xavier P, Madec G (2015) Global seasonal forecast system version 5 (GloSea5): a high-resolution seasonal forecast system. Q J Roy Meteor Soc 141:1072–1084. https://doi.org/10.1002/qj.2396

Mariotti A, Ruti PM, Rixen M (2018) Progress in subseasonal to seasonal prediction through a joint weather and climate community effort. Npj Clim Atmos Sci 1:4. https://doi.org/10.1038/s41612-018-0014-z

Materia S, Ardilouze C, Prodhomme C, Donat MG, Benassi M, Doblas-Reyes FJ et al (2022) Summer temperature response to extreme soil water conditions in the Mediterranean transitional climate regime. Clim Dyn 58:1943–1963

McKinnon K, Rhines A, Tingly M, Huybers P (2016) Long-lead predictions of Eastern United States hot days from Pacific Sea surface temperatures. Nat Geosci 9:389–394. https://doi.org/10.1038/ngeo2687

Mechoso CR, Robertson AW, Barth N, Davey MK, Delecluse P, Gent PR, Ineson S, Kirtman B, Latif M, Le Treut H, Nagai T, Neelin JD, Philander SGH, Polcher J, Schopf PS, Stockdale T, Suarez MJ, Terray L, Thual O, Tribbia JJ (1995) The seasonal cycle over the Tropical Pacific in General Circulation Models. Mon Weather Rev 123:2825–2838

Merryfield WJ, Baehr J, Batte L et al (2020) Current and emerging developments in subseasonal to decadal prediction. Bull Am Meteorol Soc 101:E869–E896. https://doi.org/10.1175/BAMS-D-19-0037.1

Mo KC, Schemm JKE, Yoo SH (2009) Influence of ENSO and the Atlantic multidecadal oscillation on drought over the United States. J Clim 22:5962–5982

Molod A, Hackert E, Vikhliaev Y, Zhao B, Barahona D, Vernieres G, Borovikov A, Kovach RM, Marshak J, Schubert S, Li Z, Lim Y-K, Andrews LC, Cullather R, Koster R, Achuthavarier D, Carton J, Coy L, Freire JLM, Longo KM, Nakada K, Pawson S (2020) GEOS-S2S version 2: the GMAO high resolution coupled model and assimilation system for seasonal prediction. J Geophy Res-Atmos 125:e2019JD031767. https://doi.org/10.1029/2019JD031767

Nakamura T, Yamazaki K, Iwamoto K, Honda M, Miyoshi Y, Ogawa Y, Ukita J (2015) A negative phase shift of the winter AO/NAO due to the recent Arctic sea-ice reduction in late autumn. J Geophys Res Atmos 120:3209–3227. https://doi.org/10.1002/2014JA020764

Nan SL, Zhao P, Chen JM (2019) Variability of summertime Tibetan tropospheric temperature and associated precipitation anomalies over the central-eastern Sahel. Clim Dyn 52:1819–1835

Nobre P, Siqueira LSP, De Almeida RAF, Malagutti M, Giarolla E, Castelã OGP, Bottino MJ, Kubota P, Figueroa SN, Costa MC, Baptista M, Irber L, Marcondes GG (2013) Climate simulation and change in the brazilian climate model. J Clim 26:6716–6732. https://doi.org/10.1175/JCLI-D-12-00580.1

Orth R, Seneviratne S (2017) Variability of soil moisture and sea surface temperatures similarly important for climate in the warm season. J Clim 30:2141–2162. https://doi.org/10.1175/JCLID-15-0567.1

Oshima K, Tachibana Y, Hiyama Y (2015) Climate and year-to-year variability of atmospheric and terrestrial water cycles in the three great Siberian rivers. J Geophys Res Atmos 120:3043–3062. https://doi.org/10.1002/2014JD02248

Pegion K, Kirtman BP, Becker E (2019) The Subseasonal Experiment (SubX): a multimodel subseasonal prediction experiment. Bull Am Meteorol Soc 100:2043–2060. https://doi.org/10.1175/BAMS-D-18-0270.1

Pu B, Fu R, Dickinson RE, Fernando DN (2016) Why do summer droughts in the Southern Great Plains occur in some La Niña years but not others? J Geophys Res Atmos 121:1120–1137

Qi X, Yang J, Xue Y, Bao Q, Wu G, Ji D (2022) Subseasonal warming of surface soil enhances precipitation over the eastern Tibetan Plateau in early summer. J Geophys Res Atmos 127:e2022JD037250

Qiu Y, Feng J, Wang J, Xue Y, Xu Z (2022) Memory of land surface and subsurface temperature (LST/SUBT) initial anomalies over Tibetan Plateau in different land models. Clim Dyn. https://doi.org/10.1007/s00382-021-05937-z

Ren X, Yang X, Chu C (2010) Seasonal variations of the synoptic-scale transient eddy activity and polar front jet over East Asia. J Clim 23:3222–3233

Ren X, Yang D, Yang X-Q (2015) Characteristics and mechanisms of the subseasonal eastward extension of the South Asian High. J Clim 28(17):6799–6822

Ren Q, Jiang X, Zhang Y, Li Z, Yang S (2021) Effects of Suppressed Transient Eddies by the Tibetan Plateau on the East Asian Summer Monsoon. J Clim 34(21):8481–8501

Robertson AW, Camargo SJ, Sobel A, Vitart F, Wang S (2018) Summary of workshop on sub-seasonal to seasonal predictability of extreme weather and climate. Npj Clim Atmos Sci 1:20178. https://doi.org/10.1038/s41612-017-0009-1

Rui M, Wang G (2011) Impact of sea surface temperature and soil moisture on summer precipitation in the United States based on observational data. J Hydrometeorol 12:1086–1099

Saha SK, Xue Y, Krishnakumar S, Diallo I, Shivamurthy Y, Nakamura T, Tang Q, Chaudhari H (2023) A dominant mode in the first phase of the Asian summer monsoon rainfall: role of antecedent remote land surface temperature. Clim Dyn. https://doi.org/10.1007/s00382-023-06709-7

Saha SK, Sujith K, Pokhrel S, Chaudhari HS, Hawra A (2017) Effect of multilayer snow scheme on the simulation of the snow: offline Noah and coupled with NCEPCFSv2. J Adv Model Earth Sy 9:271–290. https://doi.org/10.1002/2016MS000845

Sanna A, Borrelli A, Athanasiadis P, Materia S, Storto A, Navarra A, Tibaldi S, Gualdi S (2016) CMCC-SPS3: the CMCC Seasonal Prediction System 3. CMCC Research Paper (RP0285), available at: https://www.cmcc.it/wpcontent/uploads/2017/12/rp0285-csp-10-2017.pdf. Accessed 1 Jan 2023

Scaife AA, Kucharski F, Folland CK et al (2009) The CLIVAR C20C project: selected 20th century climate events. Clim Dyn 33:603–614

Seneviratne SI, Corti T, Davin EL, Hirschi M, Jaeger EB, Lehner I, Boris O, Teuling AJ (2010) Investigating soil moisture–climate interactions in a changing climate: a review. Earth Sci Rev 99(3–4):125–161. https://doi.org/10.1016/j.earscirev.2010.02.004

Shukla J, Mintz Y (1982) Influence of land-surface evapotranspiration on the earth's climate. Science 215:1498–1501

Shukla RP, Huang B, Dirmeyer PA, Kinter JL (2019) The influence of summer deep soil temperature on early winter snow conditions in Eurasia in the NCEP CFSv2 simulation. J Geophys Res Atmos 124(16):9062–9077. https://doi.org/10.1029/2019JD030279

Simmons AJ, Wallace JM, Branstator GW (1983) Barotropic wave propagation and instability, and atmospheric teleconnection patterns. J Atmos Sci 40:1363–1392

Sud YC, Shukla J, Mintz Y (1988) Influence of land surface roughness on atmospheric circulation and precipitation: a sensitivity study with a general circulation model. J Appl Meteorol 27:1036–1054

Sugimoto S, Xue Y, Sato T, Takahashi HG (2022) Influence of convective processes on Weather Research and Forecasting model precipitation biases over East Asia. Clim Dyn. https://doi.org/10.1007/s00382-022-06587-5

Takaya Y, Hirahara S, Yasuda T, Matsueda S, Toyoda T, Fujii Y, Sugiomoto H, Matsukawa C, Ishikawa I, Mori H, Nagasawa R, Kubo Y, Adachi N, Yamanaka G, Kuragano T, Shimpo A, Maeda S, Ose T (2018) Japan Meteorological Agency/Meteorological Research Institute-Coupled Prediction System version 2 (JMA/MRI-CPS2):atmosphere– land–ocean–sea ice coupled prediction system for operational seasonal forecasting. Clim Dyn 50:751–765. https://doi.org/10.1007/s00382-017-3638-5

Tang Q, Klein SA, Xie S, Lin W, Golaz J-C, Roesler EL, Taylor MA, Rasch PJ, Bader DC, Berg LK, Caldwell P, Giangrande SE, Neale RB, Qian Y, Riihimaki LD, Zender CS, Zhang Y, Zheng X (2019) Regionally refined test bed in E3SM atmosphere model version 1 (EAMv1) and applications for high-resolution modelling. Geosci Model Dev 12:2679–2706. https://doi.org/10.5194/gmd-12-2679-2019

Thompson LG, Mosley-Thompson E, Davis ME, Porter SE, Kenny DV, Lin PN (2018) Global-scale abrupt climate events and black swans: an ice-core-derived palaeoclimate perspective from Earth's highest mountains. The Himalayan cryosphere: past and present. Geol Soc Lond Spec Publ 462:7–22

Vitart F, Ardilouze C, Bonet A, Brookshaw A, Chen M, Codorean C, Hendon H (2017) The subseasonal to seasonal (S2S) prediction project database. Bull Am Meteorol Soc 98:163–173

Voldoire A, Saint-Martin D, Sénési S, Decharme B, Alias A, Chevallier M, Colin J, Guérémy J-F, Michou M, Moine M-P, Nabat P, Roehrig R, Salas y Mélia D, Séférian R, Valcke S, Beau I, Belamari S, Berthet S, Cassou C, Cattiaux J, Deshayes J, Douville H, Ethé C, Franchistéguy L, Geoffroy O, Lévy C, Madec G, Meurdesoif Y, Msadek R, Ribes A, Sanchez-Gomez E, Terray L, Waldman R (2019) Evaluation of CMIP6 DECK Experiments with CNRM-CM6-1. J Adv Model Earth Sy 11:2177–2213

Von Storch H, Zwiers FZ (1999) Statistical analysis in climate research. Cambridge University Press, Cambridge

Wallace JM, Lim GH, Blackmon ML (1988) Relationship between cyclone tracks, anticyclone tracks and baroclinic waveguides. J Atmos Sci 45:439–462

Wang B, Bao Q, Hoskins B, Wu G, Liu Y (2008) Tibetan Plateau warming and precipitation changes in East Asia. Geophys Res Lett 35:L14702

Wang M, Wang J, Duan A, Yang J, Liu Y (2019) Quasi-biweekly impact of the atmospheric heat source over the Tibetan Plateau on summer rainfall in Eastern China. Clim Dyn 53:4489–4504. https://doi.org/10.1007/s00382-019-04798-x

Woolnough SJ (2019) The Madden-Julian oscillation. In: Robertson AW, Vitart F (eds) Sub-seasonal to seasonal prediction: the gap between weather and climate forecasting. Elsevier, Amsterdam, pp 93–117

Wu GX, Liu YM, Wang TM et al (2007) The influence of mechanical and thermal forcing by the Tibetan Plateau on Asian climate. J Hydrometeorol 8:770–789

Xu X, Zhang R, Koike T, Lu C, Shi X, Zhang S, Bian L, Cheng X, Li P, Ding G (2008) A new integrated observational system over the Tibetan Plateau. Bull Am Meteorol Soc 89(10):1492–1496

Xu H, Liang X-Z, Xue Y (2022) Regional climate modeling to understand Tibetan heating remote impacts on East China precipitation. Clim Dyn. https://doi.org/10.1007/s00382-022-06266-5

Xue Y, Juang HMH, Li WP, Prince S, DeFries R, Jiao Y, Vasic R (2004) Role of land surface processes in monsoon development: East Asia and West Africa. J Geophys Res-Atmos 109:D03105. https://doi.org/10.1029/2003JD003556

Xue Y, Juang H-MH, Li W-P, Prince S, DeFries R, Jiao Y, Vasic R (2004) Role of land surface processes in monsoon development: East Asia and West Africa. J Geophys Res 109:D03105. https://doi.org/10.1029/2003JD003556

Xue Y, De Sales F, Vasic R, Mechoso CR, Prince SD, Arakawa A (2010) Global and temporal characteristics of seasonal climate/vegetation biophysical process (VBP) interactions. J Clim 23:1411–1433. https://doi.org/10.1175/2009JCLI3054.1

Xue Y, Vasic R, Janjic Z, Liu YM, Chu PC (2012) The impact of spring subsurface soil temperature anomaly in the Western U.S. on North American summer precipitation—a case study using regional climate model downscaling. J Geophys Res-Atmos 117:D11103. https://doi.org/10.1029/2012JD017692

Xue Y, De Sales F, Lau WKM, Boone A, Kim K-M, Mechoso CR, Wang G, Kucharski F, Schiro K, Hosaka M, Li S, Druyan LM, SeidouSanda I, Thiaw WM, Zeng N, Comer RE, Lim Y-K, Mahanama S, Song G, Gu Y, Hagos SM, Chin M, Schubert S, Dirmeyer P, Leung LR, Kalnay E, Kitoh A, Lu C-H, Mahowald NM, Zhang Z (2016a) West African monsoon decadal variability and drought and surface-related forcings: second West African Monsoon Modeling and Evaluation Project Experiment (WAMME II). Clim Dyn 47:3517–3545

Xue Y, Oaida CM, Diallo I, Neelin JD, Li S, De Sales F, Gu Y, Robinson DA, Vasic R, Yi L (2016b) Spring land temperature anomalies in northwestern US and the summer drought over Southern Plains and adjacent areas. Environ Res Lett 11:044018. https://doi.org/10.1088/1748-9326/11/4/044018

Xue Y, Ma Y, Li Q (2017) Land–climate interaction over the Tibetan Plateau in Oxford Research Encyclopedia of Climate Science. Oxford Press, Oxford. https://doi.org/10.1093/acrefore/9780190228620.013.59

Xue Y, Diallo I, Li W, Neelin JD, Chu PC, Vasic R, Guo W, Li Q, Robinson DA, Zhu Y, Fu C, Oaida CM (2018) Spring land surface and subsurface temperature anomalies and subsequent downstream late spring-summer droughts/floods in North America and East Asia. J Geophys Res Atmos 105:5001–5019. https://doi.org/10.1029/2017JD028246

Xue Y, Boone AA, Yao T (2019a) Remote effects of high elevation land surface temperature on S2S precipitation prediction—international workshop of first phase of GEWEX/GASS LS4P Initiative and TPEMIP. GEWEX News 29(1):14–16. International GEWEX Project Office, Silver Spring

Xue Y, Lau WKM, Yao T, Boone AA (2019b) Remote effects of Tibetan Plateau Spring Land surface temperature on global summer precipitation and its S2S prediction: second workshop on LS4P and TPEMIP. GEWEX News 29(1):8–10. International GEWEX Project Office, Silver Spring

Xue Y, Yao T, Boone AA, Diallo I, Liu Y, Zeng X, Lau WKM, Sugimoto S, Tang Q, Pan X, Van Oevelen PJ, Klocke D, Koo M-S, Lin Z, Takaya Y, Sato T, Ardilouze C, Saha SK, Zhao M, Liang X-Z, Vitart F, Li X, Zhao P, Neelin JD, Guo W, Yu M, Qian Y, Shen SSP, Zhang Y, Yang K, Leung R, Yang J, Qiu Y, Brunke MA, Chou SC, Ek M, Fan T, Guan H, Lin H, Liang S, Materia S, Nakamura T, Qi X, Senan R, Shi C, Wang H, Wei H, Xie S, Xu H, Zhang H, Zhan Y, Li W, Shi X, Nobre P, Qin Y, Dozier J, Ferguson CR, Balsamo G, Bao Q, Feng J, Hong J, Hong S, Huang H, Ji D, Ji Z, Kang S, Lin Y, Liu W, Muncaster R, Pan Y, Peano D, Rosnay PD, Takahashi HG, Tang J, Wang G, Wang S, Wang W, Zhou X, Zhu Y (2021) Impact of initialized land surface temperature and snowpack on subseasonal to seasonal prediction project, phase I (LS4P-I): organization and experimental design. Geosci Model Dev 14:1–30

Xue Y, Diallo I, Boone AA, Yao T, Zhang Y, Zeng X, Neelin JD, Lau WKM, Pan Y, Liu Y, Pan X, Tang Q, Van Oevelen PJ, Sato T, Koo M-S, Materia S, Shi C, Yang J, Ardilouze C, Lin Z, Xin Q, Nakamura T, Saha SK, Senan R, Takaya Y, Wang H, Zhang H, Zhao M, Nayak HP, Chen Q, Feng J, Brunke MA, Fan T, Hong S, Nobre P, Peano D, Qin Y, Vitart F, Xie S, Zhan Y, Klocke D,

Leung R, Li X, Ek M, Guo W, Balsamo G, Bao Q, Chou SC, Rosnay PD, Lin Y, Zhu Y, Qian Y, Zhao P, Tang J, Liang X-Z, Hong J, Ji D, Ji Z, Qiu Y, Sugimoto S, Wang W, Yang K, Yu M (2022) Spring land temperature in Tibetan plateau and global-scale summer precipitation—initialization and improved prediction. Bull Am Meteorol Soc 103(12):E2756–E2767. https://doi.org/10.1175/BAMS-D-21-0270.1,E2756-E2767

Yanai M, Li C, Song Z (1992) Seasonal heating of the Tibetan Plateau and its effects on the evolution of the Asian summer monsoon. J Meteorol Soc Jpn 70:319–351

Yang Z, Zhang J, Wu L (2019) Spring soil temperature as a predictor of summer heatwaves over north western China. Atmos Sci Lett 20:e887. https://doi.org/10.1002/asl.887

Yang J, Chen H, Song Y, Zhu S, Zhou B, Zhang J (2021) Atmospheric circumglobal teleconnection triggered by spring land thermal anomalies over West Asia and its possible impacts on early summer climate over Northern China. J Clim 34:5999–6021. https://doi.org/10.1175/JCLI-D-20-0911.1

Yang Z, Zhang J, Liu Y, Li K (2022) The substantial role of May soil temperature over Central Asia for summer surface air temperature variation and prediction over Northeastern China. Clim Dyn. https://doi.org/10.1007/s00382-022-06360-8

Yasunari T, Kitoh A, Tokioka T (1991) Local and remote responses to excessive snow mass over Eurasia appearing in the northern spring and summer climate: a study with the MRI GCM. J Meteorol Soc Jpn 62:473–487

Ye D (1981) Some characteristics of the summer circulation over the Qinghai-Xizang (Tibet) Plateau and its neighbourhood. Bull Am Meteorol Soc 62(1):14–19. https://doi.org/10.1175/1520-0477(1981)062%3c0014:SCOTSC%3e2.0.CO;2

Zeng N, Neelin JD, Lau K-M, Tucker CJ (1999) Enhancement of inter-decadal climate variability in the Sahel by vegetation interaction. Science 286:1537–1540

Zhao P, Zhou Z, Liu J (2007) Variability of Tibetan spring snow and its associations with the hemispheric extratropical circulation and East Asian summer monsoon rainfall: an observational investigation. J Clim 20(15):3942–3955. https://doi.org/10.1175/JCLI4205.1

Zhao P, Xu X, Chen F, Guo X, Zheng X, Liu L, Hong Y, Li Y, La Z, Peng H, Zhong L (2018) The third atmospheric scientific experiment for understanding the earth–atmosphere coupled system over the Tibetan Plateau and its effects. Bull Am Meteorol Soc 99(4):757–776

Zhao Y, Sun R, Xie Z, Duan A (2022) Upper-troposphere saddle-like response to springtime surface sensible heating over the Tibetan Plateau: Combined effect from baroclinic and barotropic process. J Geophys Res Atmos 127:e2021JD036002. https://doi.org/10.1029/2021JD036002

Zhu C, Liu B, Li L, Ma S, Jiang N, Yan Y (2022) Progress and prospects of research on subseasonal to seasonal variability and prediction of the East Asian monsoon. J Meteorol Res 36(5):677–690. https://doi.org/10.1007/s13351-022-2059-5

Authors and Affiliations

Yongkang Xue[1] · **Ismaila Diallo[1,31]** · **Aaron A. Boone[2]** · **Yang Zhang[3]** · **Xubin Zeng[4]** · **William K. M. Lau[5]** · **J. David Neelin[1]** · **Tandong Yao[6]** · **Qi Tang[7]** · **Tomonori Sato[8]** · **Myung-Seo Koo[9]** · **Frederic Vitart[10]** · **Constantin Ardilouze[2]** · **Subodh K. Saha[11]** · **Stefano Materia[12,13]** · **Zhaohui Lin[14]** · **Yuhei Takaya[15]** · **Jing Yang[16]** · **Tetsu Nakamura[8]** · **Xin Qi[16]** · **Yi Qin[7,17]** · **Paulo Nobre[18]** · **Retish Senan[10]** · **Hailan Wang[19]** · **Hongliang Zhang[20]** · **Mei Zhao[21]** · **Hara Prasad Nayak[1]** · **Yan Pan[3]** · **Xiaoduo Pan[6]** · **Jinming Feng[14]** · **Chunxiang Shi[22]** · **Shaocheng Xie[7]** · **Michael A. Brunke[4]** · **Qing Bao[23]** · **Marcus Jorge Bottino[18]** · **Tianyi Fan[16]** · **Songyou Hong[9,24]** · **Yanluan Lin[17]** · **Daniele Peano[12]** · **Yanling Zhan[14]** · **Carlos R. Mechoso[1]** · **Xuejuan Ren[3]** · **Gianpaolo Balsamo[10]** · **Sin Chan Chou[18]** · **Patricia de Rosnay[10]** · **Peter J. van Oevelen[25]** · **Daniel Klocke[26]** · **Michael Ek[27]** · **Xin Li[6]** · **Weidong Guo[3]** · **Yuejian Zhu[19]** · **Jianping Tang[3]** · **Xin-Zhong Liang[28]** · **Yun Qian[29]** · **Ping Zhao[30]**

✉ Yongkang Xue
yxue@geog.ucla.edu

1   University of CA-Los Angeles, Los Angeles, CA 90095, USA

2   CNRM, Université de Toulouse, Météo-France, CNRS, Toulouse, France

3   School of Atmospheric Sciences, Nanjing University, Nanjing, China

4   University of Arizona, Tucson, USA

5   Earth System Science Interdisciplinary Center, University of Maryland, College Park, MD, USA

6   Institute of Tibetan Plateau Research, Chinese Academy of Sciences (CAS), Beijing, China

7   Lawrence Livermore National Laboratory, Livermore, USA

8   Hokkaido University, Sapporo, Japan

9   Korea Institute of Atmospheric Prediction Systems, Seoul, South Korea

10   European Centre for Medium-Range Weather Forecasts, Reading, UK

11   Indian Institute of Tropical Meteorology, Pune, India

12   Climate Simulation and Prediction, Fondazione Centro Euro-Mediterraneo sui Cambiamenti Climatici, Bologna, Italy

13   Barcelona Supercomputing Centre, Barcelona, Spain

14   Institute of Atmospheric Physics, CAS, Beijing, China

15   Meteorological Research Institute, Japan Meteorological Agency, Tsukuba, Japan

16   Beijing Normal University, Beijing, China

[17] Tsinghua University, Beijing, China

[18] National Institute for Space Research (INPE), Cachoeira Paulista, Brazil

[19] National Center for Environmental Prediction, College Park, MD, USA

[20] National Meteorology Center, CMA, Beijing, China

[21] Bureau of Meteorology, Melbourne, Australia

[22] National Meteorological Information Center, China Meteorological Administration (CMA), Beijing, China

[23] LASG, Institute of Atmospheric Physics, CAS, Beijing, China

[24] NOAA/ESRL and University of Colorado/CIRES, Boulder, CO, USA

[25] International GEWEX Project Office, George Mason University, Fairfax, USA

[26] Max Planck Institute for Meteorology, Hamburg, Germany

[27] National Center for Atmospheric Research, Boulder, USA

[28] University of Maryland, College Park, MD, USA

[29] Pacific Northwest National Laboratory, Richland, WA 99352, USA

[30] Chinese Academy of Meteorological Sciences, China Meteorological Administration, Beijing, China

[31] The Pennsylvania State University, University Park, PA 16802, USA